Parallel density scanned Adaptive Kriging to improve local Tsunami Hazard Assessment for coastal infrastructures

F. Di Maio[1], M. Belotti[1], M. Volpe[2], J.Selva[3], E. Zio[1,4]

[1] Energy Department, Politecnico di Milano, Via La Masa 34, Milano, 20156, Italy

[2] Istituto Nazionale di Geofisica e Vulcanologia, Via di Vigna Murata 605, 00143 Roma, Italy

3 Istituto Nazionale di Geofisica e Vulcanologia, Via Franceschini, 31, 40100 Bologna, Italy

[4] MINES ParisTech, PSL Research University, CRC, Sophia Antipolis, France

* Corresponding author: francesco.dimaio@polimi.it

Abstract

Seismic Probabilistic Tsunami Hazard Assessment (SPTHA) aims at calculating the probability that seismically induced tsunami waves exceed a specific height, in a given time span and over a specific region (i.e. regional SPTHA) or site (i.e. local SPTHA). To account for the uncertainty of the possible sources, SPTHA must integrate the results of a large number of computationally demanding tsunami simulations

In this work, we innovatively use Parallel density scanned Adaptive Kriging (P-ds AK) to overcome the computational efficiency challenge of local SPTHA within a framework that consists in modelling/retrieving the full spectrum of possible earthquake triggering events at the regional level, filtering sources not relevant for the target, adopting a clustering procedure to select "representative scenarios" for inundation modelling, and, finally, adopt P-ds AK to identify the clusters centroids that most influence the hazard intensity (i.e., wave height) in the areas of interest.

This approach is applied in the area of the oil refinery located in Milazzo (Italy). The application shows a consistent reduction of the number of high-resolution tsunami simulations required for the evaluation of the hazard curves over a set of inland Point of Interest (PoIs), either concentrated in one specific area or distributed along the coast.

Keywords: Seismic Probabilistic Tsunami Hazard Assessment (SPTHA); Hazard Curve; Parallel density scanned Adaptive Kriging (P-ds AK); Oil & Gas Industry; Refinery.

Acronyms

AK	Adaptive Kriging	**NaTech**	Natural Hazard Triggering Technological Disaster**s**
AKMCS	Adaptive Kriging Monte Carlo Sampling	**PoI**	Point of Interest
P-ds AK	Parallel density-based Adaptive Kriging	**SPTHA**	Seismic Probabilistic Tsunami Hazard Assessment
DoE	Design of Experiment	**MinPts**	Minimum number of points in a cluster
ET	Event Tree	**I/O**	Input/Output

Symbols

$\underline{\boldsymbol{\psi}}$	Tsunami intensity threshold	$\sigma_{\widehat{G}}$	Standard deviation of a metamodel prediction
$\boldsymbol{\psi}_{\boldsymbol{z}}$	Tsunami intensity in $\boldsymbol{z}$	$\boldsymbol{x}^{\boldsymbol{c}}$	Centroid earthquake parameters
$\boldsymbol{\Delta T}$	Exposure time	$\mu_{\widehat{G}(x)_z}$	Mean value of a metamodel prediction
$\boldsymbol{z}$	Point of Interest (PoI)	$\boldsymbol{\Phi}$	Normal (Gaussian) distribution
$\boldsymbol{\lambda}$	Mean annual frequency	$\boldsymbol{\eta}(\underline{\boldsymbol{\psi}})_{\boldsymbol{z}}$	Convergence index of the metamodel built for PoI $\boldsymbol{z}$ and intensity $\underline{\psi}$
$\boldsymbol{\Theta}$	Set of alternative models	$\widehat{\boldsymbol{P}}_{\boldsymbol{e}}$	Probability of exceedance
$\boldsymbol{\vartheta}$	Alternative model	$\widehat{\boldsymbol{P}}_{\boldsymbol{m}}$	Probability of misclassifying
$\boldsymbol{x}$	Seismic scenario parameters	$\boldsymbol{I}$	Total number of iterations
$\boldsymbol{J}$	Number of seismic features	$\boldsymbol{i}$	Generic iteration
$\boldsymbol{j}$	Seismic feature index	$\boldsymbol{U}$	U learning function
$\boldsymbol{\sigma}_{\boldsymbol{x}}$	Seismic scenario	$\boldsymbol{K}_{\boldsymbol{i}}$	Number of density-based clusters
$\boldsymbol{\Sigma}$	Space of possible seismic scenarios	$\boldsymbol{k}_{\boldsymbol{i}}$	Density-based cluster
$\boldsymbol{s}$	Generic index of seismic scenario	$\boldsymbol{D}$	Distance between two inputs
$\boldsymbol{S}$	Total number of seismic scenarios	ξ	Radius of density based clustering
$\boldsymbol{G}$	Performance function	$\boldsymbol{v}$	Generic index of a candidate
$\widehat{\boldsymbol{G}}$	Surrogate of the performance function	$\boldsymbol{Pr}$	Probability
$\boldsymbol{g}$	Tsunami inundation model	$\widehat{\boldsymbol{P}}_{\boldsymbol{e}}$	Probability of exceedance
$\boldsymbol{Z}$	Total number of Points of Interest	$\widehat{\boldsymbol{P}}_{\boldsymbol{m}}$	Probability of misclassification
$\boldsymbol{A}$	Number of intensities that are considered for a hazard curve construction	ρ	Sphere radius
$\boldsymbol{a}$	Index of an intensity of a natural hazard	$\varphi_{\boldsymbol{AB}}$	Sphere angle between A and B
$\boldsymbol{N}$	Number of total filtered seismic scenarios	ϕ	Latitude
$\boldsymbol{M}$	Number of alternative models	θ	Longitude
$\boldsymbol{p}$	Generic index offshore wave height	β	Trend coefficients of Kriging approximation

P	Number of offshore wave height	$\hat{\beta}$	Trend coefficients least square estimates
ψ_p	Offshore wave height	δ	Hyperparameters of the Kriging model
N_1	Number of filtered seismic scenarios after Filter H	O	Kriging metamodel Information matrix
N_2	Number of filtered seismic scenarios after Filter P	L	Gaussian likelihood function
$\psi_{thresh.}$	Wave threshold for Filter P	T	Number of arbitrary functions of Kriging trend
$\lambda_{thresh.}$	Earthquake mean annual occurence threshold	R	Correlation matrix
C	Number of clusters and number of centroids	r	element of the cross correlations vector
c	Cluster and centroid index	q	Generic PoI
f	Gaussian distributed Kriging prediction	Var	Variance

1 Introduction

Accidents triggered by natural hazards (i.e., earthquakes, floods, tsunamis) pose significant threats to safety-critical systems, like oil and gas and nuclear facilities, because they may lead to losses of hazardous materials with potentially tremendous impact on the environment and the population. These technological accidents caused by natural hazards are known as Natural Hazard Triggering Technological Disasters (NaTech) (Moreno et al., 2019; Mesa-Gomez et al., 2020; Khakzad et al., 2020; Lan et al., 2022). Industrial facilities located in coastal areas are exposed to tsunami NaTech and the associated potential flooding, resulting in damage or collapse of buildings, tanks or other equipments, possibly causing the release of contaminants (Antonioni et al., 2015; Cruz et al., 2009; Landucci et al., 2012). The Niigata (1964) and Tohoku (2011) earthquakes and tsunamis, for example, resulted in oil spread from an oil refinery plant (Iwabuchi et al., 2006) and radioactive release of material from a nuclear power plant (Sato & Lyamzina, 2018), respectively.

To manage tsunami threat, tsunami hazard and risk methodologies have been developed through time to quantify and manage the tsunami hazard and the potential consequent risks (Grezio et al., 2017; Kameshwar et al., 2019; Behrens et al., 2021; Selva et al., 2021 for a review on the state-of-the-art tsunami hazard and risk assessments). For Natech, these studies may help identifying the preventive and mitigative countermeasures for such calamitous events.

Early on, “worst credible”/ “worst case” scenarios approaches have been adopted (Tinti et al., 2011; Tonini et al., 2011; El-Hussain et al., 2018). These consist in the postulation of conservative and deterministic scenarios, which are then simulated by high-resolution codes to verify the response of the system and its safety barriers. For example, in Cruz et al. (2009), a worst case analysis of tsunamis impacting an oil refinery is reported. In Prasad (2012) and Lo (2014), applications to a nuclear power plant are described. However, these approaches have proven to be limited in modelling seismic sources as well as tsunamis due to the large uncertainty given by the scarcity of tsunami observations (Geist & Parsons, 2014).

To rationally address the problem, Seismic Probabilistic Tsunami Hazard Assessment (SPTHA) has been proposed for the explicit treatment of the large spectrum of uncertainty relative to seismic triggering events and tsunami propagation (Selva et al., 2021). SPTHA aims to estimate the probability that a tsunami intensity measure ψ_z (e.g. height of the wave) exceeds a threshold value $\underline{\psi}$ at a given Point of Interest (PoI) z and within a time span ΔT (exposure time): each tsunami is assumed to be generated by a seismic scenario σ_x belonging to a space of possible seismic scenarios ($\sigma_x \in \Sigma$), characterized by parameters $x = [x_1, \dots, x_j, \dots, x_J]$ and occurring with annual frequency $\lambda(\sigma_x)$; Assuming a homogeneous Poisson process for the probability of exceedance $\underline{\psi}$, we can write:

$$P_e = \Pr\left(\psi_z \geq \underline{\psi}; \Delta T\right) \approx 1 - exp\left(-\lambda\left(\psi_z \geq \underline{\psi}\right) \Delta T\right) \quad (1)$$

where $\lambda\left(\psi_z \geq \underline{\psi}\right)$ is the mean annual frequency of occurence of a tsunami of intensity $\psi_z \geq \underline{\psi}$ at location z, and

$$\lambda\left(\psi_z \geq \underline{\psi}\right) = \int_{\Sigma} \lambda(\sigma_x) Pr\left(\psi_z \geq \underline{\psi} | \sigma_x\right) d\sigma_x \quad (2)$$

Eq. (2) integrates over the scenarios the annual frequency $\lambda(\sigma_x)$ of the seismic source σ_x and the probability $Pr\left(\psi_z \geq \underline{\psi} | \sigma_x\right)$ that the generated tsunami wave would exceed $\underline{\psi}$. Considering, without loss of generality but for the sake of simplicity, a set of S discretized seismic scenarios σ_{x_s} ($s = 1, \dots, S$), Eq (2) can be evaluated as:

$$\lambda\left(\psi_z \geq \underline{\psi}\right) \approx \sum_{s}^{S} \lambda(\sigma_{x_s}) Pr\left(\psi_z \geq \underline{\psi} | \sigma_{x_s}\right). \quad (3)$$

The hazard curve for the PoI z is defined by quantifying the probability of at least one exceedance in the time span ΔT for a set of $\underline{\psi}$: i.e, $Pr\left(\psi_z \geq \underline{\psi}; \Delta T\right)$:

$$Pr\left(\psi_z \geq \underline{\psi}; \Delta T\right) \approx 1 - exp\left(-\sum_s^S \lambda(\sigma_{x_s}) Pr\left(\psi_z \geq \underline{\psi} | \sigma_{x_s}\right) \Delta T\right). \quad (4)$$

For sake of simplicity, hazard curves can be reported without this conversion to probability, simply plotting $\underline{\psi}\ vs.\ \lambda\left(\psi_z \geq \underline{\psi}\right)$. Such values are numerically equivalent for sufficiently small mean annual rates (e.g. < 0.01).

Alternative models may be set for quantifying both $\lambda(\sigma_{x_s})$ and $Pr\left(\psi_z \geq \underline{\psi} | \sigma_{x_s}\right)$ selected from a set of alternative models $\Theta = \left\{\vartheta : \vartheta \Longrightarrow \lambda(\sigma_x), Pr\left(\psi_z \geq \underline{\psi} | \sigma_{x_s}\right)\right\}$, allowing for the quantification of the uncertainty on the hazard curves (epistemic uncertainty).

The annual frequency $\lambda(\sigma_x)$ is associated to a specific seismic scenario σ_x obtained by discretizing the space of the source parameters x, for example adopting an Event Tree (ET) (Basili et al., 2021). The $Pr\left(\psi_z \geq \underline{\psi} | \sigma_x\right)$, instead, must be calculated by means of tsunami simulations.

Regional SPTHA computational challenge is typically addressed by simulating tsunami propagation only offshore and using simplified relationships between the water elevation offshore and the one at the shoreline and/or the maximum inundation height (Gailler et al., 2018; Glimsdal et al., 2019; Løvholt et al.,

2016). For example, the first long-term PTHA from earthquake-induced tsunamis for the NEAM (North-eastern Atlantic, the Mediterranean, and connected seas) region, the NEAM Tsunami Hazard Model 2018 (NEAMTHM18; Basili et al., 2021), considers millions of seismic sources and estimates the inundation probability at regional scale, based on offshore tsunami propagation and subsequent onshore extrapolation. Alternatively, the uncertainty propagation can be carried out by breaking down the typically high-dimensional problem into several low-dimensional ones, one for each level of the hierarchy in the computational workflow. For example, in (Tbandeh et al., 2022), on a regional risk and resilience analysis of a community, it is shown an adaptive refinement of uncertainty propagation to identify the influential uncertain input data and computational sub-models.

On the other hand, local SPTHA requires high-resolution inundation simulations for the specific sites, forcing analysts (to date) to either explore large HPC resources (e.g., Tonini et al., 2021) or to reduce the number of simulations in order to make the assessment computationally manageable (Lorito et al. 2015; Volpe et al., 2019) In Lorito et al. (2015) and Volpe et al. (2019) the authors have proposed a filtering procedure that reduces the number of seismic scenarios to be simulated with the non-linear inundation model. This procedure considers a clustering technique to aggregate seismic scenarios based on the similarity of the offshore tsunami waves in front of the target site, building the inundation hazard curves by simulating only the centroids of the clusters

In this work, we present a novel approach to reduce the number of scenarios required for SPTHA, based on the use of Adaptive Kriging (AK). The approach extends that of Volpe et al. (2019). AK is a fast-running surrogate metamodel introduced first by Echard et al. (2011). It is here adopted to mimic the behavior of the computationally demanding tsunami inundation simulator, after training on a set of evaluations by the full scope model, which make up the Design of Experiment (DoE). In AK, the DoE is progressively enriched heuristically to drive the metamodel to simulate inundations only for critical values of the parameters. More precisely, given an Input/Output (I/O) representation $\psi_z = g(x)$ of the tsunami inundation model $g(x)$ producing a hazard intensity ψ_z at a location z, the specific combination of input seismic parameters values x that make the seismic scenario critical (i.e, the resulting output value is larger than the predefined threshold, $\psi_z = g(x) \geq \underline{\psi}$) is pursuit. To do this, a performance function $G\left(x|\underline{\psi}\right)_z = \underline{\psi} - g(x)$ is defined and the AK builds a surrogate function $\hat{G}\left(x|\underline{\psi}\right)_z$ by collecting iteratively the I/O patterns $\{x, \psi(x)_z\}$ most affecting the neighborhood of the limit state function $G\left(x|\underline{\psi}\right)_z = 0$ (Turati et al., 2017; Wang & Wang, 2013). This allows obtaining an accurate estimate of the probability of exceedance $Pr\left(G\left(x|\underline{\psi}\right)_z \leq 0|\sigma_x\right)\left(= Pr\left(\psi_z \geq \underline{\psi}|\sigma_x\right)\right)$, for each seismic scenario σ_x.

In literature, various AK approaches have been proposed, all initiated by the Adaptive Kriging Monte Carlo Sampling (AKMCS) (Echard et al., 2011) that has been successively refined and revisited in many works, such as: (Turati et al., 2017; Xiaobo Zhang et al., 2021; L. Puppo et al., 2021). Parallel density scanned Adaptive Kriging (P-ds AK) has been recently introduced in (Teixeira et al., 2020) to allow the

parallelization of the evaluations of the model output within an unsupervised procedure that i) enhances the exploration of the input parameter values, overcoming the typical overfitting limitations of traditional AKMCS that often rely on training sets of DoEs not enough sparse and diverse (Jian et al., 2017; Sun et al., 2017), ii) allows for a limited number of DoEs, overcoming the unfeasible prediction of very low probability values, such as $Pr\left(\psi_z \geq \underline{\psi}|\sigma_x\right)$, with a very small number of patterns available (Xufang Zhang et al., 2019), and iii) guarantees acceleration of the convergence of the Kriging predictions (Teixeira et al., 2020).

The approach is applied to a real case study for constructing Z hazard curves for a set of Z $(= 1, \dots, z, \dots, Z)$ PoIs in the area of the oil refinery site located in Milazzo (Italy), each developed for a series of A $(= 1, \dots, a, \dots, A)$ tsunami intensities $\underline{\psi}_a$. The results are compared with those presented in Volpe et al. (2019) for the same site, and show large computational savings with respect to two relevant use cases: inundation at coastal points (i.e, an extended area of tanks of the refinery exposed to the tsunami wave) and at a set of narrow points (i.e, around specific tanks of the refinery).

The paper is organized as follows: in Section 2, the novel AK-based SPTHA for the construction of a hazard curve is described; in Section 3 the case study is presented; in Section 4, the results of the application of the AK-based SPTHA and its comparison with methods of literature are discussed to illustrate the advantages of the proposed AK-based SPTHA; finally, in Section 5, conclusions are drawn.

2 Methodology

2.1 P-ds-AK-based SPTHA

The proposed P-ds-AK-based SPTHA stands on the procedure presented in Volpe et al. (2019) and sketched in *Figure* 1 (for convenience, the definition of steps is slightly modified with respect to Volpe et al, 2019). The procedure is described in the following. Steps 1-3 are in common to both the original and the new algorithms.

Step 1) A set of S seismic scenarios triggering a tsunami event is considered. The mean annual rate of occurrence of a tsunami triggering event, i.e., of a seismic scenario σ_x, is modelled by an ET. Each parameter x_j $(j = 1, \dots, J)$ of a scenario is sampled from the corresponding logically ordered conditional probability $Pr\left(x_j|x_1, \dots, x_{j-1}\right)$ described by the ET (Selva et al. 2016) and multiplied by the mean annual rate λ of the generic event in the seismic zone in which the scenario is originated. The mean annual rate of the scenario is:

$$\lambda\left(\sigma_x\right) = Pr\left(x_j|x_1, \dots, x_{j-1}\right) \dots \cdot Pr(x_1)\lambda \quad (5)$$

For each sampled seismic scenario σ_x, a set of values of the annual frequency of occurrence $\lambda(\sigma_x)$ is obtained by the set of ϑ_m $\left(\vartheta_m \Longrightarrow \lambda(\sigma_x)\right)$ alternative models $\Theta = \{\vartheta_1, \vartheta_2, \dots, \vartheta_m, \dots, \vartheta_M\}$, representing the epistemic uncertainty of the seismic source (Selva et al., 2016).

Step 2) For each scenario σ_x, the tsunami wave is propagated by means of regional-scale low-resolution numerical tsunami simulations, from the earthquake epicenter to P selected offshore points, in which the set $\{\psi(x)_p\}_{p=1,\dots P}$ of maximum wave heights is computed.

Step 3) Filtering and clustering are applied to the whole set of scenarios, in order to reduce the number of local-scale high-resolution numerical simulations required.

3a) A subset of N_1 ($N_1 < S$) scenarios are selected by FILTER H (H = height): in what follows, only earthquakes σ_x leading to an offshore maximum wave height $\psi(x)_p$ larger than a certain threshold $\psi_{threshold}$ are considered (i.e, σ_x: $max_{p=1,\dots,P}(\psi(x)_p) > \psi_{threshold}$).

3b) A subset of $N = N_2$ ($N_2 < N_1 < S$) scenarios are selected by FILTER P (P = probability): in what follows, only earthquakes σ_x with mean annual frequency of occurrence $\lambda(\sigma_{x,\vartheta})$, considering the mean of the epistemic uncertainty defined as the mean of the M alternative models $\left(\lambda(\sigma_{x,\vartheta}) = \frac{\sum_m^M \lambda(\sigma_{x,\vartheta_m})}{M}\right)$, larger than a certain threshold $\lambda_{threshold}$ are considered (i.e, σ_x: $\lambda(\sigma_{x,\vartheta}) > \lambda_{threshold}$).

3c) a k-medoids-clustering analysis (Kaufman L. and Rousseeuw, 2009) is performed to identify C clusters of scenarios of characteristics x_i and x_y (i $\neq y$, $i = 1, \dots, N$ and $y = 1, \dots N$) with large similarity in the offshore tsunami profile at P=11 offshore control points (Eq. 6):

$$d(x_i, x_y) = \left[1 - \frac{2\sum_p^{11} \psi(x_i)_p \psi(x_y)_p}{\sum_p^{11} (\psi(x_i)_p{}^2 + \psi(x_y)_p^2)}\right] \quad (6)$$

By doing so, each scenario σ_x is assigned to a *c*-th cluster and represented by the *c*-th centroid σ_{x^c}, with parameters x^c. Note that a different metric can be used when near-field sources are treated (Volpe et al., 2019).

Step 4) The original procedure, at this point, consists in running an inundation non-linear shallow water model C times, with parameters x^c $(c = 1, \dots, C)$ to simulate the inundation induced by the C centroid scenarios σ_{x^c} and the maximum wave heights $\{\psi(x^c)_z\}_{z=1,\dots,Z}$ at the PoIs $z = 1, \dots, Z$ are computed. For each scenario σ_x belonging to the *c*-th cluster, $\psi(x)_z$ is taken equal to $\psi(x^c)_z$ for every PoI z, and $Pr\left(\geq \underline{\psi} | \sigma_x\right)$ to $Pr\left(\psi_z \geq \underline{\psi} | \sigma_{x^c}\right)$. Uncertainty on propagation is neglected, and an identify function is adopted (see Grezio et al. 2017): if $\psi(x)_z > (<) \underline{\psi}$, then $Pr\left(\psi_z \geq \underline{\psi} | \sigma_x\right) = 1\ (= 0)$. This is a common practice for local SPTHA, even if important uncertainty may exist about inundation model (Griffin et al., 2015; Song and Goda, 2021; Tonini et al. 2021). All these terms are finally substituted in eq. 1 and 3, and the total hazard is aggregated for each target point.

The new procedure modifies the final step of the original procedure (Figure 2), integrating numerical simulations and hazard aggregation into a loop in which P-ds AK selects the scenarios to model. More specifically, we use a P-ds AK method that allows to further reduce the computational cost by selecting a subset of meaningful centroids x^c, among the C available, to estimate $Pr\left(\psi_z \geq \underline{\psi} | \sigma_x\right)$ for each seismic scenario σ_x, as shown in Figure 2. This allows: i) wide exploration of the input parameter values ii) limited

number of DoEs for the prediction of very low probability, such as $Pr\left(\psi_z \geq \underline{\psi}|\sigma_x\right)$, with an overall iii) acceleration of the convergence for the hazard aggregation. The P-ds AK based procedure is used to build Z hazard curves for a set of $Z\ (=1,\dots,z,\dots,Z)$ PoIs, each developed for a series of $A\ (=1,\dots,a,\dots,A)$ intensities $\underline{\psi}_a$; for the z-th PoI and the a-th intensity $\underline{\psi}_a$, a Kriging metamodel is built to predict $Pr\left(\psi_z \geq \underline{\psi}; \Delta T\right)$, resulting in the construction of ZxA metamodels.

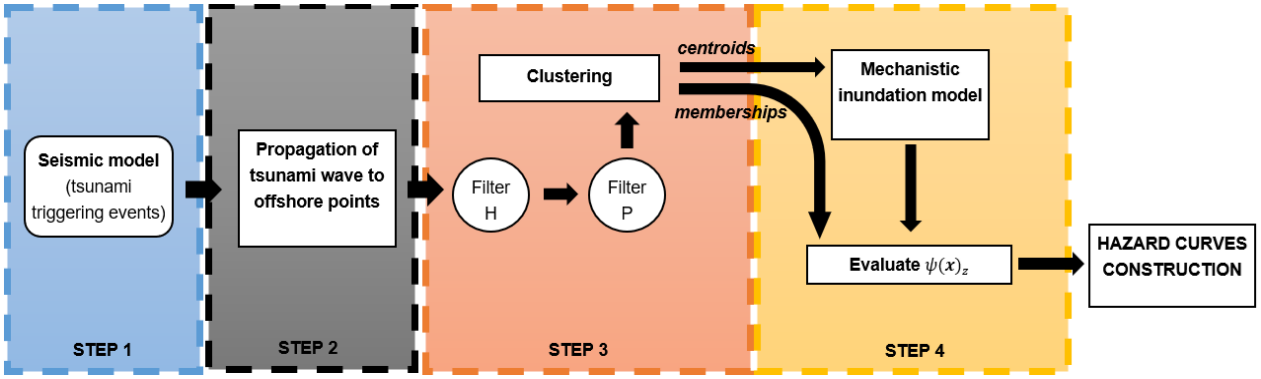

Figure 1: Flowchart for SPTHA as in Volpe et al. (2019)

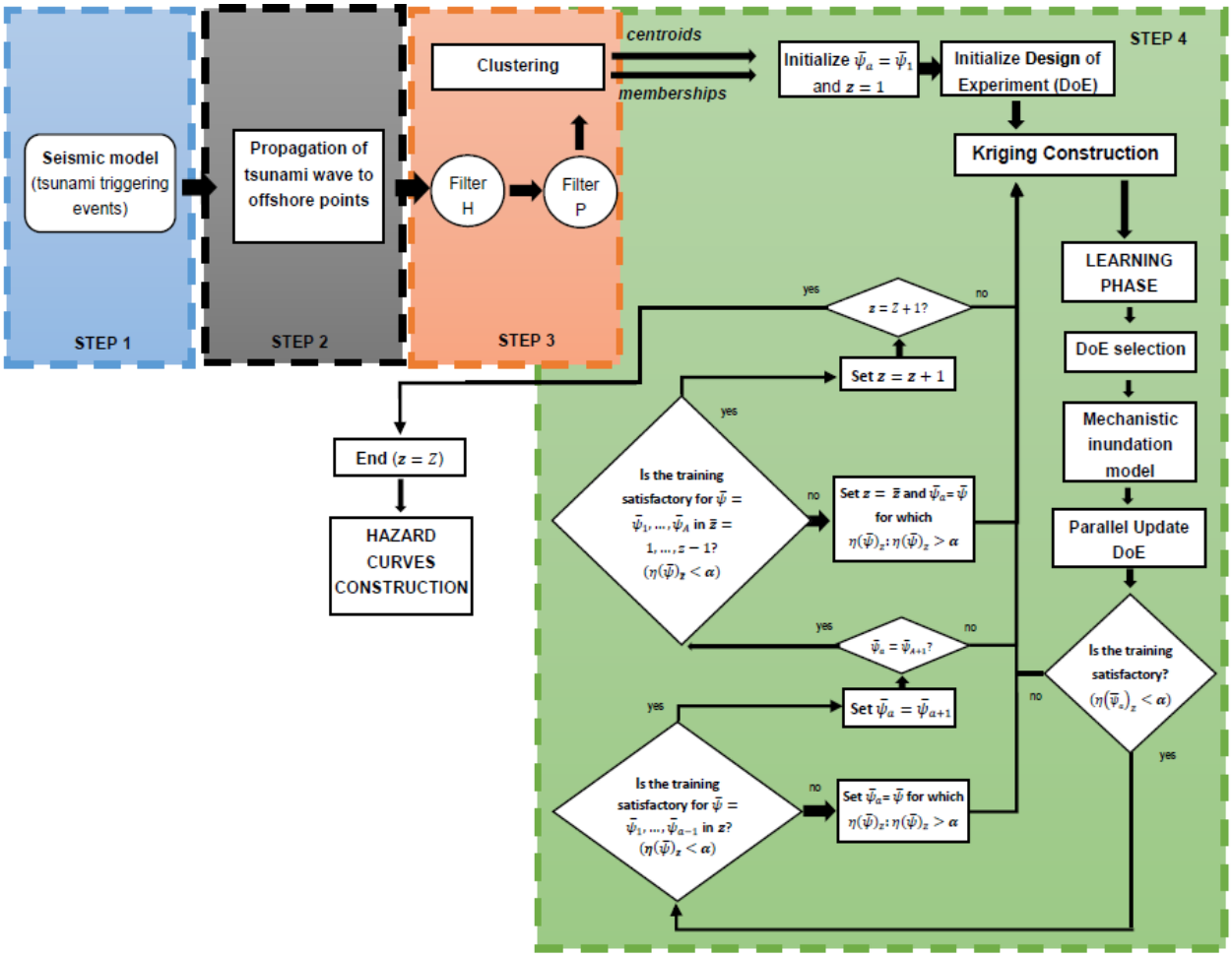

Figure 2: Flowchart for AK based SPTHA

To develop a Kriging metamodel for a specific PoI z and a specific intensity measure $\underline{\psi}$, a random set of I/O patterns is taken from the availables centroids, called DoEs,$\{x_{DOE},\ \psi(x_{DOE})_z\}$, and the algorithm is able to build a surrogate $\hat{G}\left(x|\underline{\psi}\right)_z$ of the performance function $G\left(x|\underline{\psi}\right)_z = \underline{\psi} - g(x)$. Then, for a generic input, the metamodel predicts a Gaussian distributed output $f(\hat{G}\left(x|\underline{\psi}\right)_z)$ (Turati et al., 2017):

$$f(\hat{G}\left(x|\underline{\psi}\right)_z) \sim \Phi\left(\mu_{\hat{G}\left(x|\underline{\psi}\right)_z},\ \sigma^2{}_{\hat{G}\left(x|\underline{\psi}\right)_z}\right). \quad (7)$$

The probability $\hat{P}_e(x|\underline{\psi})$ of exceedance of $\underline{\psi}$ for the seismic scenario σ_x is:

$$\hat{P}_e(x|\underline{\psi}) = \frac{1}{2\pi\,\sigma_{\hat{G}\left(x|\underline{\psi}\right)_z}} \int_{-\infty}^{0} exp\left(-\frac{(\hat{G}\left(x|\underline{\psi}\right)_z - \mu_{\hat{G}\left(x|\underline{\psi}\right)_z})^2}{2\,\sigma^2{}_{\hat{G}\left(x|\underline{\psi}\right)_z}}\right) d\hat{G}\left(x|\underline{\psi}\right)_z \quad (8)$$

and the probability $\hat{P}_m(x|\underline{\psi})$ of prediction misclassification for the input x to exceed the measure $\underline{\psi}$ as:

$$\hat{P}_m(x|\underline{\psi}) = \frac{1}{2\pi\,\sigma_{\hat{G}\left(x|\underline{\psi}\right)_z}} \int_{-\infty}^{0} exp\left(-\frac{\left(\hat{G}\left(x|\underline{\psi}\right)_z - \left|\mu_{\hat{G}\left(x|\underline{\psi}\right)_z}\right|\right)^2}{2\,\sigma^2{}_{\hat{G}\left(x|\underline{\psi}\right)_z}}\right) d\hat{G}(x)_z. \quad (9)$$

The AK algorithm is able to enrich the DoE, for the selected PoI z and intensity measure $\underline{\psi}$, iteratively identifying the I/O patterns $\{x,\ \psi(x)_z\}$ that most affect the neighborhood of the limit state function $G\left(x|\underline{\psi}\right)_z = 0$, based on the prediction made by the surrogate function $\hat{G}\left(x|\underline{\psi}\right)_z$. The iteration holds until a defined metric $\eta(\underline{\psi})_z$ approaches a convergence criterion $\eta(\underline{\psi})_z < \alpha$. In particular, to reduce the overall computational costs of the procedure, the DoE is simultaneously enriched for all the ZxA metamodels built to simulate the response of the tsunami $\{\psi(x)_z\}_{z=1,\dots,Z}$ for the Z PoIs.

Note that the addition of simulations for new I/O pattern $\{x,\ \psi(x)_z\}$ to the DoE set of Kriging metamodels may affect their performance; therefore, convergence is verified with respect to:

I. $\eta(\underline{\psi}_a)_z$: convergence of the current specific metamodel built for PoI z and intensity $\underline{\psi}_a$).

II. $\left\{\eta(\underline{\psi}_1)_z, \dots, \eta(\underline{\psi}_{a-1})_z\right\}$: convergence of the ensemble of specific metamodels built for the set of intensities $\underline{\psi}_{1,\dots,}\underline{\psi}_{a-1}$ in PoI z, i.e. the set of metamodels aimed at building the hazard curve of PoI z. The addition to the DoE of a seismic scenario σ_x critical for the current metamodel can be, in principle, critical also for the metamodels built over the same PoI z and with similar intensities to the current $\underline{\psi}_a$.

III. $\left\{\eta(\underline{\psi}_a)_1\right\}_{a=1,\dots,A}, \dots, \left\{\eta\left(\underline{\psi}_a\right)_{z-1}\right\}_{a=1,\dots,A}$: convergence of the ensemble of specific metamodels built for the set of A $(= 1, \dots, a, \dots, A)$ intensities $\underline{\psi}_a$ in PoIs $1, \dots, z-1$, i.e. the set of metamodels for building the hazard curve of PoIs $1, \dots, z-1$.

In practice, the P-ds AK iterative $(i = 1, \dots, I)$ procedure starts by setting a list of Z $(= 1, \dots, z, \dots, Z)$ PoIs and of A $(= 1, \dots, a, \dots, A)$ intensities $\underline{\psi}_a$. Then, the procedure is configured as follows:

1. Kriging construction: a Kriging metamodel is constructed using the available I/O training set $\{x_{DOE},\ \psi(x_{DOE})_z\}^i$, of increasing dimensions as i increases; the metamodel accuracy is expected to improve, specifically, in proximity of the limit state function $G\left(x|\underline{\psi}_a\right)_z = 0$.

2. Learning phase:
   a. Metamodel Evaluation: Kriging metamodel is used to evaluate the surrogate function output corresponding to the N seismic scenarios σ_x with parameters $(x_1, \dots, x_N)$: $f(\hat{G}(x_1|\underline{\psi}_a)_z), \dots, f(\hat{G}(x_N|\underline{\psi}_a)_z)$.
   b. U function calculation: among the N available seismic scenarios patterns, a subset of N_{cand} best candidates are selected on the basis of their U learning function values:

$$U(x) = \frac{|\mu_{\hat{G}\left(x|\underline{\psi}_a\right)_z}|}{\sigma_{\hat{G}\left(x|\underline{\psi}_a\right)_z}} \tag{10}$$

   where $\mu_{\hat{G}\left(x|\underline{\psi}_a\right)_z}$ is the predicted mean value and $\sigma_{\hat{G}\left(x|\underline{\psi}_a\right)_z}$ the related estimation error of $f(\hat{G}\left(x|\underline{\psi}_a\right)_z)$. The $U(x)$ value represents the distance, normalized to the standard deviation, of the metamodel prediction from $G\left(x|\underline{\psi}_a\right)_z = 0$: a candidate x with low $U(x)$ can be of interest either because it can be a set of seismic parameters whose event would result in a ψ close to the threshold region ($\mu_{\hat{G}\left(x|\underline{\psi}_a\right)_z} = 0$), or because it can be a set of seismic parameters whose event would result in a very uncertain scenario, not yet explored ($\sigma_{\hat{G}\left(x|\underline{\psi}_a\right)_z}$ large).
   c. Density-based clustering: a density-based clustering procedure is performed to cluster the subset N_{cand} of candidates σ_x, based on the features x, into K_i $(k_i = 1, \dots, K_i)$ clusters.The algorithm is based on the definition of a radius ξ and a minimum number of points in the k_i-th cluster (MinPts): if within ξ, more than MinPts are found for each x, the x becomes a core point of the k_i-th cluster; if not enough MinPts are in its neighbourhood but among the adjacent points are present core points, then x is assigned to that cluster and is called reachable. Finally, x is an outlier if is further than ξ with respect to all core points.

3. DoE selection: the $\hat{P}_m$ of Eq. (9) is evaluated for all the $x \in k_i$-th cluster. Then, the x scoring the maximum $\hat{P}_m$, namely $x_{DOE}^{k_i} = argmax(\hat{P}_m(x^{k_i}))$, is added to the DoE; the procedure is repeated for all the K_i clusters, resulting in the collection of a set $\left\{x_{DOE}^{k_i}\right\}_{k_i=1,\dots,K_i}$.

4. Mechanistic inundation model: the output $\{\psi(x_{DOE}^{k_i})_z\}_{z=1,\dots,Z}$ $(k_i = 1, \dots, K_i)$ corresponding to the K_i new training patterns $\{x_{DOE}^{k_i}\}_{k_i=1,\dots,K_i}$ is taken equal to the mechanistic inundation model simulation $\{\psi(x^c)_z\}_{z=1,\dots,Z}$ of the centroid x^c of the c-th cluster which they belong to.

5. Parallel update DoE: the DoEs of the ZxA metamodels are enriched simultaneously. In the end, each K_i I/O sequence $\{x_{DOE}^{k_i}, \psi(x_{DOE}^{k_i})_z\}_{k_i=1,\dots,K_i}$ is added to the I/O training set of each metamodel constructed for PoI $(= 1, \dots, Z)$.

6. Convergence check (level I): the Kriging construction continues iteratively from Phases 1 to 5 until:

$$\eta(\underline{\psi}_a)_z = \frac{\frac{1}{N}\sum_n^N \hat{P}_m(x_n|\underline{\psi}_a)}{\frac{1}{N}\sum_n^N \hat{P}_e(x_n|\underline{\psi}_a)} < \alpha \qquad (11)$$

where α is called accuracy level (i.e, the mean of the misclassification probability $\hat{P}_m$ is α-times smaller than the mean exceedance probability $\hat{P}_e$).

7. Convergence (level II): for the metamodels based on the intensity measures $\underline{\psi} = \underline{\psi}_1, \dots, \underline{\psi}_{a-1}$ in PoI z, the convergence criterions $\left\{\eta(\underline{\psi}_1)_z, \dots \eta(\underline{\psi}_{a-1})_z\right\}$ are calculated, and:
    a. If $\exists\, \eta(\underline{\psi})_z: \eta(\underline{\psi})_z > \alpha$, Kriging construction is repeated from Phases 1 to 5 for the metamodels based on the intensities $\underline{\psi}$ and PoI z for which the convergence criterion $\eta(\underline{\psi})_z > \alpha$.
    b. Else if $\nexists\, \eta(\underline{\psi})_z: \eta(\underline{\psi})_z > \alpha$, the intensity is set to $\underline{\psi}_a = \underline{\psi}_{a+1}$ and:
        i. If $\underline{\psi}_a \neq \underline{\psi}_{A+1}$, return to Phase 1.
        ii. If $\underline{\psi}_a = \underline{\psi}_{A+1}$, go to Phase 8.

8. Convergence check (level III): for the metamodels based on the intensity measures $\underline{\psi} = \underline{\psi}_1, \dots, \underline{\psi}_A$ in PoIs $\underline{z} = 1, \dots, z-1$, the convergence criterions $\left\{\eta(\underline{\psi}_1)_1, \dots \eta(\underline{\psi}_A)_1\right\}, \dots,$ $\left\{\eta(\underline{\psi}_1)_{z-1}, \dots \eta(\underline{\psi}_A)_{z-1}\right\}$ are calculated, and:
    a. If $\exists\, \eta(\underline{\psi})_{\underline{z}}: \eta(\underline{\psi})_{\underline{z}} > \alpha$, Kriging construction is repeated from Phases 1 to 5 for the metamodels based on the PoIs $\underline{z}$ and intensities $\underline{\psi}$ whose convergence criterion $\eta(\underline{\psi})_z > \alpha$.
    b. If $\nexists\, \eta(\underline{\psi})_{\underline{z}}: \eta(\underline{\psi})_{\underline{z}} > \alpha$, the PoI is set to $z = z + 1$ and:
        i. If $z \neq Z + 1$, return to Phase 1.
        ii. If $z = Z + 1$, end of the procedure.

To summarize, the P-ds AK based procedure aims at building a set of ZxA Kriging metamodels. Each one is trained from a set of $\Delta + \sum_1^I K_i \left(= \Delta + \underline{K}\right)$ I/O patterns $\{x_{DOE}, \psi(x_{DOE})_z\}$ and provides a

Gaussian distributed prediction for each seismic scenario σ_x of the probability of exceeding $\underline{\psi}$ in a PoI z, namely $\hat{P}_e\left(x|\underline{\psi}\right) = Pr\left(\psi_z \geq \underline{\psi}|\sigma_x\right)$. To estimate the hazard curves at target points, i.e. $Pr\left(\psi_z \geq \underline{\psi}; \Delta T\right)$, from Eq. (4), the hazard aggregation is performed by summing the individual probabilities combined by their annual frequency over all the N seismic scenarios σ_x, i.e., $\sum_n^N \lambda\left(\sigma_{x_n}\right) \hat{P}_e(x_n)$. The associated uncertainty is often assumed as Beta-distributed (Marzocchi et al., 2015) which, locally, i.e., with respect to each seismic scenario σ_x, can be approximated by Normal distributions (Sinharay, 2010). This justifies the use of AK to estimate $\hat{P}_e\left(x|\underline{\psi}\right) = Pr\left(\psi_z \geq \underline{\psi}|\sigma_x\right)$ and approximate it to a Gaussian distribution (see Eq. (7)).

3 Case study

The approach described in Section 2, is applied for the construction of tsunami hazard curves for the site of the oil refinery located in Milazzo, on the north-eastern coast of Sicily, Italy. The results are benchmarked with those discussed in Volpe et al. (2019).

3.1 Seismic events characterization and tsunami modelling

The regional seismicity model adopted in Volpe et al. (2019) has been developed in the framework of the EU project ASTARTE (http://www.astarte-project.eu). Without loss of generality, we limit our study to the sources in the far field, i.e. sources which do not generate significant coseismic displacement at the target site. Such dataset consists of the $S = 1684017$ far-field crustal scenarios σ_x. To account for the epistemic uncertainty, a set of M =100 alternative models ϑ_m were considered. For our purposes, we will focus on the mean hazard curve, as well as the 15th and 85th percentiles.

To produce local SPTHA, a set of P=11 offshore control points on the 50m isobath in front of Milazzo have been selected. The propagation of the seismic-induced tsunami waves to the control points was done applying the Tsunami-HySEA code, a nonlinear hydrostatic shallow-water multi-GPU code based on a mixed finite-difference–finite-volume method (Macias et al., 2017). Each scenario was obtained by means of a linear combination of precalculated tsunami waveforms produced by Gaussian-shaped unitary sources (Molinari et al., 2016).

Among the S available scenarios, $N = 32715$ scenarios were identified as most significative for the target site, after having applied two filters: FILTER H ($max_{p=1,\dots,P}\left(\psi(x)_p\right) > 1$ m off-shore of Milazzo) and the FILTER P ($\lambda\left(\sigma_{x,\vartheta}\right) > 10^{-5} yr^{-1}$). These N scenarios were clustered in $C = 613$ clusters, by the k-medoids clustering explained in Section 2.1. This configuration has been adopted for including tsunami hazard in the stress test methodology developed for the EU project STREST (http://www.strest-eu.org/), (Argyroudis et al., 2020).

In Volpe et al. (2019), these *N* scenarios were fed to the Tsunami-HySEA code for local high-resolution inundation modelling. Here, only the most relevant centroids x^c selected by the P-ds-AK-based procedure among the C clusters available, are used and compared to the full set of simulations.

3.2 Kriging input pre-processing

The models adopted to simulate the seismic-triggered tsunamis to calculate ψ_z use J =11 $(x_1, \dots, x_j, \dots, x_J)$ input parameters for characterizing the seismic triggering events σ_x (i.e, Longitude, Latitude, water depth of the Cell, Magnitude, Length, Width, Strike, Dip, Rake, Slip and depth of the baricenter of the fault) (Volpe et al., 2019).

The development of Kriging for such high dimensional problems can be prohibitive (Bouhlel & Martins, 2017), calling for an input set pre-processing of the input variables. An expert-based feature selection has suggested to consider 6 inputs from the 11 available (the spherical coordinates (L, φ_{AB}), the magnitude of the earthquake (Magnitude), the focal parameters (Strike, Dip and Rake) and 2 further parameters: the expected value and the variance of the offshore heights $\psi(x)_p$ measured at the 50 m isobath, given by:

$$E[\psi(x)_p] = \underline{\Psi(x)}_p = \frac{\sum_p \quad \psi(x)_p}{P} \tag{12}$$

$$Var[\psi(x)_p] = \frac{1}{11}\sum_p \quad (\psi(x)_p - \underline{\Psi(x)}_p)^2. \tag{13}$$

Note that L and φ_{AB} refer to the source-target distance and longitude angle difference, respectively, of a PoI A of coordinates {ρ, ϕ_A, θ_A} with the seismic epicenter B, of coordinates {ρ, ϕ_B, θ_B}, located on a sphere (earth) of center O and radius ρ, with ϕ and θ being the Latitude and Longitude, respectively (*Figure 3*):

$$L = \rho\, arccos(\, sen(\theta_A)(\theta_B) \, + cos(\theta_A)cos(\theta_B)cos\,(\varphi_{AB})\,) \tag{14}$$

$$\varphi_{AB} = \varphi_A - \varphi_B \tag{15}$$

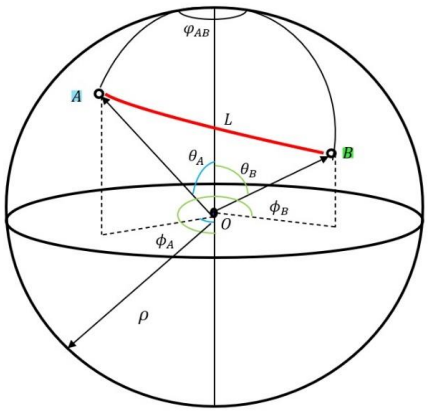

Figure 3: the spherical coordinate system

The angle φ_{AB} is used also considering the E-W coastal configuration at target and the spatial characterization of sources. Other source-target configurations may lead to change the list of parameters to be used to efficiently characterize seismic sources in input to kriging.

3.3 Metamodel construction

Following the approach described in Section 2.1, for each PoI z and intensity $\underline{\psi}_a$:

1. Kriging construction: to the best author's knowledge, no general recommendations exist to sample the initial DoE from a pre-formatted Input setting. Considering that a space filling design is needed (H. Liu et al., 2018), we follow the DoE setting called "2^J factorial design" (Raymond H. Myers, Douglas C. Montgomery, 2016): the idea is to set a DoE consisting in the combination of lowest and largest values for each feature x_j, which gives 2^J samples. The initial DoE training has been generated by Monte Carlo sampling of $\Delta = 2^8 = 256$ DoE samples and the corresponding simulation results are collected (i.e, the simulation of the centroids of the clusters which the input belongs to).
2. Learning phase:
    a. Metamodel Evaluation: the software GAUSSIAN PROCESS REGRESSION AND CLASSIFICATION toolbox version 4.2 (form Carl Edward Rasmussen and Hannes Nickisch and available at http://www.gaussianprocess.org/gpml/code/matlab/doc/) has been used to fit the Kriging metamodel to the training set of N seismic scenarios, with standard settings (Rui Teixeira, 2020):
        - Trend type: *constant*
        - Family of correlation functions: anisometric squared exponential covariance function
        - Estimation method: *Maximum likelihood.*
    b. U function calculation: among the N available patterns, a subset of $N_{cand} = 4000$ best candidates are selected on the basis of their U learning function values.
    c. Density-based clustering: the density-based clustering groups the subset of $N_{cand} = 4000$ candidates into K_i $(k_i = 1, \dots, K_i)$ clusters. In this work, MinPts is set equal to $J + 1 = 9$ and ξ to $min\,(max\,(D))$, where $D = [D_1, \dots, D_v, \dots, D_{N_{cand}=4000}]$ and $D_v = min\left(\sqrt{\sum_j^J x_j^v - x_j^{h \neq v}}\right)$ with $h = v = [1, \dots, N_{cand} = 4000]$ (in line with (Teixeira et al., 2020)).
3. DoE selection: from every k-th cluster retrieved, the seismic scenario $x_{DOE}^{k_i} = argmax(\hat{P}_m(x^{k_i}))$ is added to the DoE, resulting in the collection of a set $\left\{x_{DOE}^{k_i}\right\}_{K_i\,(k_i=1,\dots,K_i)}$.

4. Mechanistic inundation model: the mechanistic inundation model simulation is run for the centroids of the K new training patterns $\{x_{DOE}^{k}\}_{K_i\ (k_i=1,\dots,K_i)}$.
5. Parallel update DoE: K_i I/O sequence $\{x_{DOE}^{k_i},\ \psi(x_{DOE}^{k_i})_z\}_{k_i=1,\dots,K_i}$ are added to the I/O training set of each metamodel constructed for a PoI $(= 1, \dots, z, \dots, Z)$.
6. Convergence check – level I: to guarantee consistent results of the convergence criterion $\eta(\underline{\psi}_a)_z$ introduced in Eq (11), the accuracy level α is set to 0.1 (in line with (Teixeira et al., 2020)).
7. Convergence check – level II: evaluation of convergence criterions $\left\{\eta(\underline{\psi}_1)_z, \dots \eta(\underline{\psi}_{a-1})_z\right\}$ is performed.
8. Convergence check – level III: evaluation of convergence criterions $\left\{\eta(\underline{\psi}_1)_1, \dots \eta(\underline{\psi}_A)_1\right\}, \dots,$ $\left\{\eta(\underline{\psi}_1)_{z-1}, \dots \eta(\underline{\psi}_A)_{z-1}\right\}$ is performed.

4 Results

The metamodel-based P-ds AK framework introduced in Sections 2 and 3 has been applied for the construction of the hazard curves for two case studies: a set of narrow PoIs, distributed around few specific tanks belonging to the Milazzo refinery, and a set of coastal PoIs covering the entire refinery. The results are shown in terms of annual frequency $\lambda\left(\psi_z \geq \underline{\psi}\right)$, and benchmarked with those presented in Volpe et al. (2019).

4.1 Narrow PoIs

A set of narrow PoIs are selected ($z = 1, 2, 3, 4, 5, 6, 7, 8, 9$, *Figure* 4), around a group of 3 neighbour tanks. Without loss of generality, this case study is considered significant to show the benefit of the P-ds AK based SPTHA in planning effective preventive and recovery strategies of NaTech scenarios, strongly affecting the equipment and safety systems of spatially concentrated facilities (Mebarki et al., 2016).

Figure 4: narrow PoIs

Figures 5 to 8 show some examples of the obtained mean hazard curves (without loss of generality, for PoI $z = 1, 2, 3, 4$ respectively): our results are reported with continuous blue lines, whereas those obtained in (Volpe et al., 2019) with dashed red lines. In particular, the exceedance annual rates $\lambda\left(\psi_z \geq \underline{\psi}\right)$ for each PoI are shown, and the error bars corresponding to the 15th and 85th percentiles of the epistemic uncertainty are plotted.

Note that the results in (Volpe et al., 2019) have been obtained with the run of $C = 613$ centroids simulations $\psi(x^c)_z$, each one taking approximately 30 [min] with 3 GPUs (i.e., the computational time is equal to 30 [min]*613 runs of the code=19390 [min]), whereas the P-ds AK-based SPTHA results have been obtained running only $C = 280$ centroids simulations $\psi(x^c)_z$ (i.e., the computational time is equal to 80 [min] (for the Pds-AK training) + 30 [min]*280 runs of the code =8400 [min], with a saving of about half of the time).

More precisely, as shown in *Table 1*, the initial DoE of $\Delta = 256$ seismic scenarios σ_x, belonging to a total of $C = 36$ clusters (with the corresponding centroids $\{x^c\}_{c=1,\dots,36}$ and $\psi(x^c)_z$), has been iteratively enriched with a total of $\underline{K} = 358$ seismic scenarios σ_x, belonging to $C = 244$ different clusters (with the corresponding centroids $\{x^c\}_{c=1,\dots,244}$ and $\psi(x^c)_z$).

	Pds-AK based SPTHA		Volpe et al. (2019)	
	Number of calls of seismic scenarios σ_x	Number of corresponding centroids (C)	Number of calls of seismic scenarios σ_x	Number of corresponding centroids (C)
Initial DoE (Δ)	256	36	/	/
Added DoE ($\underline{K}$)	358	244	/	/
Total DoE	614	280	32715	613

Table 1: summary of the DoE and calls for narrow PoIs

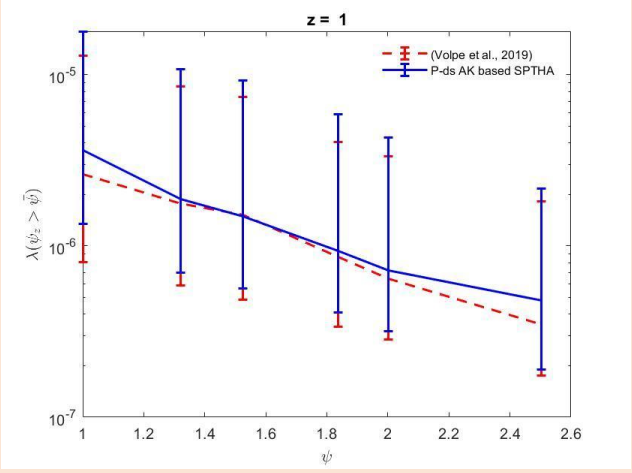

Figure 5: hazard curve for z=1

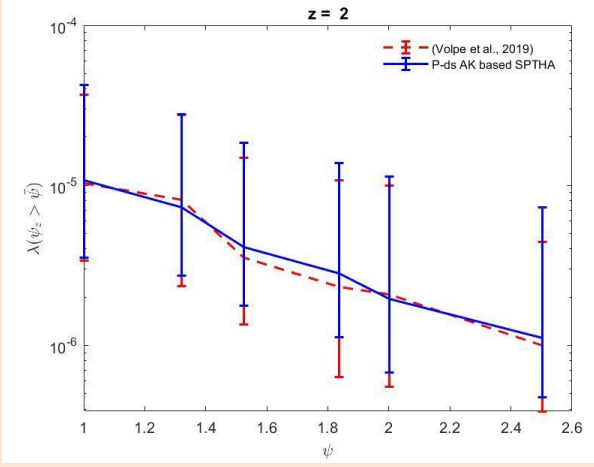

Figure 6: hazard curve for z=2

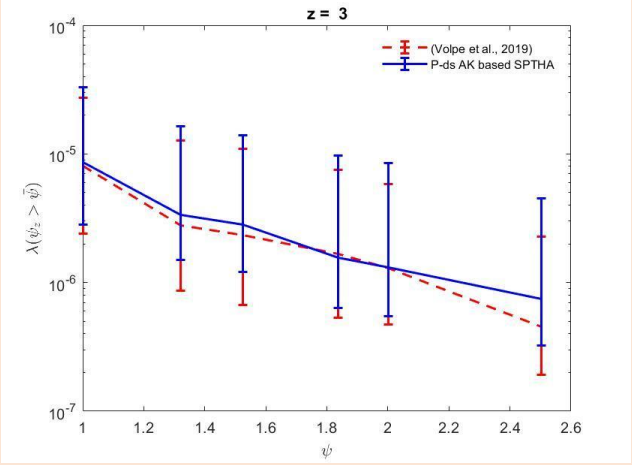

Figure 7: hazard curve for z=3

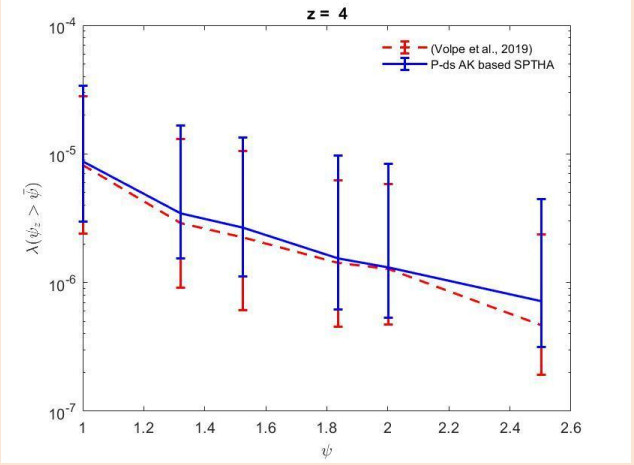

Figure 8: hazard curve for z=4

The overall results of the proposed Pds-AK based approach show a good agreement with the results in (Volpe et al., 2019) (Root Mean Squared Error (RMSE) equal to [4.66E-7, 1.46E-6, 1.13E-6, 1.0E-6, 1.50E-6, 1.15E-6, 1.38E-6, 1.66E-6, 1.70E-6] for $z = 1, 2, 3, 4, 5, 6, 7, 8, 9$, respectively). Central values show a slight tendency toward overestimation, which results however well inside the epistemic uncertainty bounds. The estimation of uncertainty is overall quite accurate too, without clear trends toward over/underestimation. Notably, an important reduction in the computational cost is observed, with $C = 280$ simulations involved with respect to $C = 613$ involved in (Volpe et al., 2019).

Note that the decrease in the number of centroids simulations $\psi(x^c)_z$ has been enabled by the P-ds AK identification of the most critical seismic scenarios σ_x; i.e, those scenarios whose parameters x_j ($j = 1, \dots, J$) would lead the simulation in the neighborhood of the limit state function $G\left(x|\underline{\psi}\right)_z = 0$. To highlight this, the distributions of the input parameters L, φ_{AB}, Strike, Dip and Rake, $E[\psi(x)_p], Var[\psi(x)_p]$ for all the available seismic scenarios (upper left), the initial DoE (upper right) and the added DoE (bottom) are plotted In *Figures* 9 to 16, respectively.

In *Figure 9* it can be seen that the P-ds AK has enriched the DoE with only those seismic events whose epicenter is, on average, close to the PoI (i.e. source-target distance L between 50 and 200 km, leaving out the evaluation sources with larger L); in *Figure* 10 it can be seen that the P ds-AK has enriched the DoE with only seismic scenarios whose φ_{AB}, the difference in longitude between the Milazzo refinery and the epicenter (see Figure 3), is small (i.,e, φ_{AB} between 0° and 0.03°) neglecting larger values of φ_{AB}. In other words, the P-ds AK allowed concentrating on the events in front of the target coast, for which also relatively smaller change would imply differences for the hazard results.

In *Figure 11* the distribution of magnitudes is shown: the P-ds AK procedure enriched the DoE with scenarios with relatively high Magnitude, in the interval 7.5 and 8.

Figure 12 shows that the DoE is enriched with scenarios σ_x whose Rake angle is of 90° and -90°. Contrarily, no changes in the DoE distribution are seen in *Figure 13* for Strike angle and *Figure* 14 for Dip angle.

Finally, in *Figures* 15-16, it can be seen that the P-ds AK enriched the DoE with σ_x with high $E[\psi(x)_p]$, with a maximum around 8 meters, and high $Var[\psi(x)_p]$.

In conclusion, we can state that it is more likely that seismic scenarios in the neighborhood of $G\left(x|\underline{\psi}\right)_z = 0$ are close to (low L) and in front of (low φ_{AB}) the site, with magnitude between 7.5 and 8 and with Rake angles of 90° and -90°, involving a large tsunami with a quite variable profile offshore to the target point. On the other hand, we can claim that, among all the available inputs, Strike and Dip angles can be neglected for building the P-ds AK metamodels.

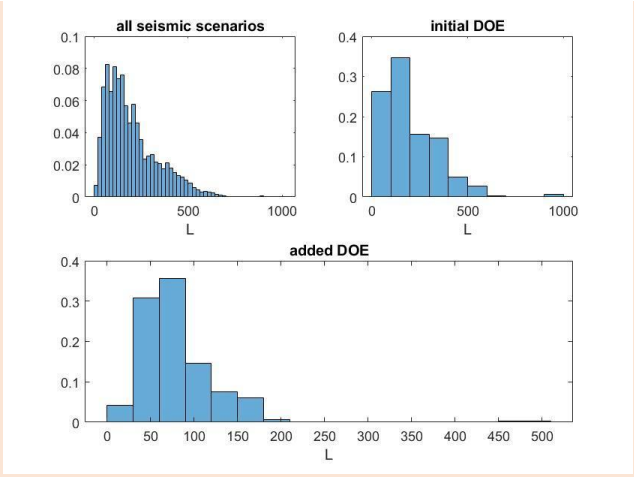

Figure 9: distributions of source-target distance L

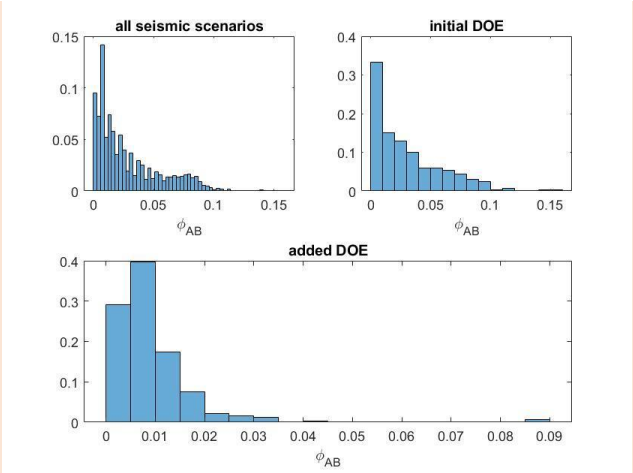

Figure 10: distributions of longitude difference φ_{AB}

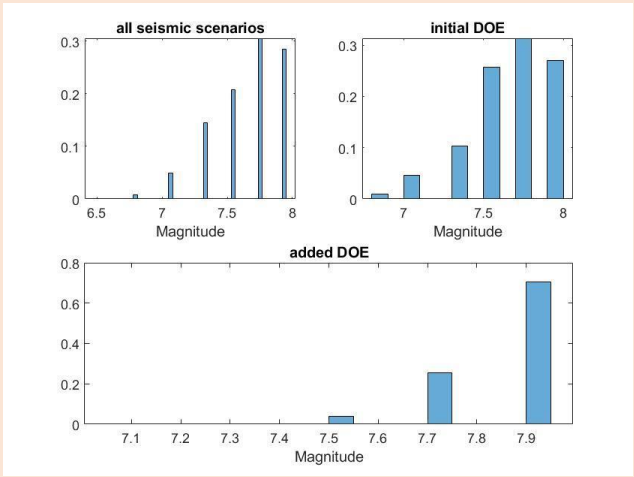

Figure 11: distributions of Magnitude

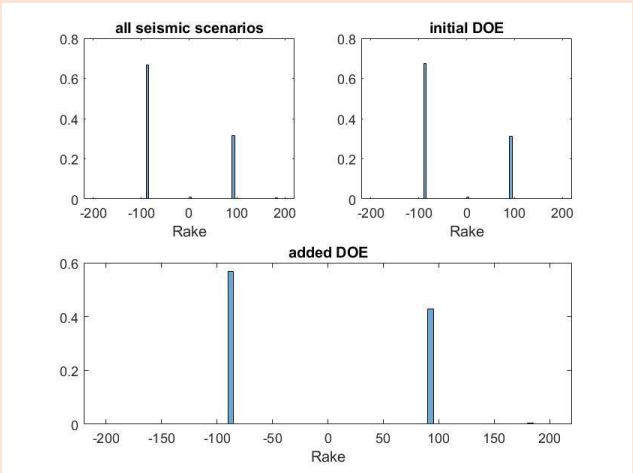

Figure 12: distributions of Rake

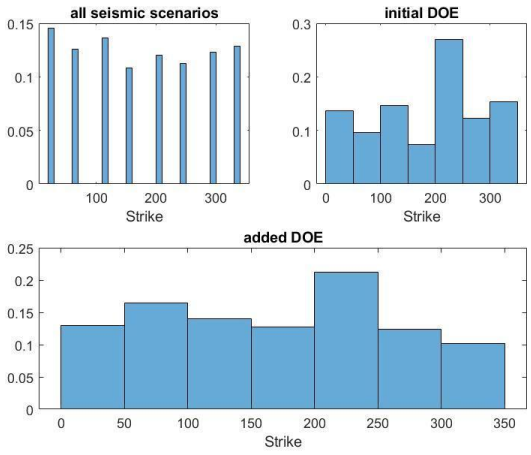

Figure 13: distributions of Strike

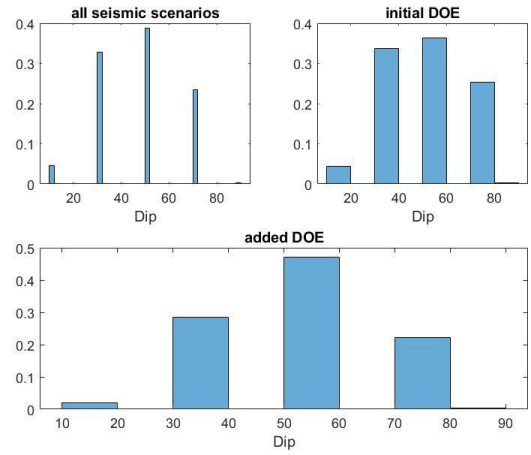

Figure 14: distributions of Dip

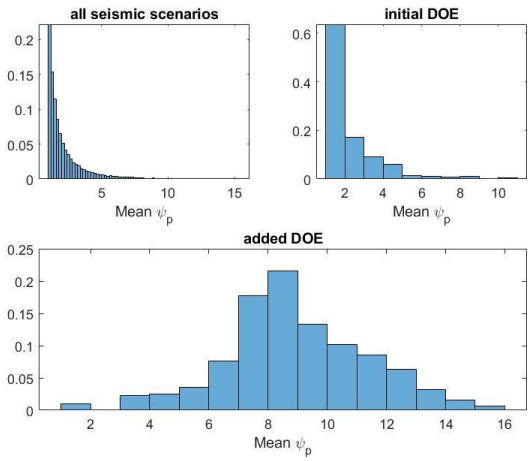

Figure 15: distributions of $\boldsymbol{E}[\boldsymbol{\psi}(\boldsymbol{x})_{\boldsymbol{p}}]$

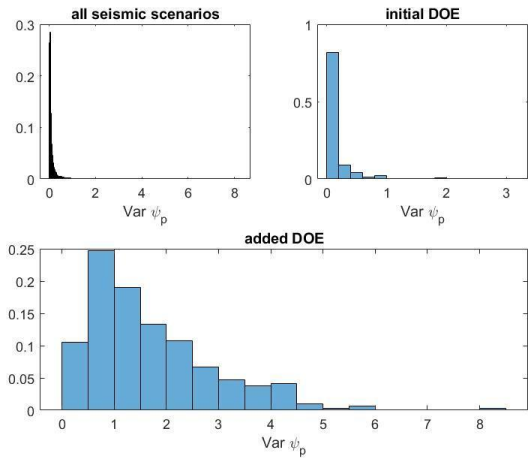

Figure 16: distributions of $\boldsymbol{Var}[\boldsymbol{\psi}(\boldsymbol{x})_{\boldsymbol{p}}]$

To further characterize these encouraging results, we analyze the classification performance of the metamodel. Without loss of generality, we restrict to PoIs $z = 2, 5, 8$, the ones in seafront position with respect to tanks. Considering $Pr\left(\psi_z \geq \underline{\psi}|\sigma_x\right) = 1$ or $Pr\left(\psi_z \geq \underline{\psi}|\sigma_x\right) = 0$ if $\mu_{\hat{G}(x)_z} < 0 (> 0)$, if we compare the P-ds AK estimate $\hat{G}\left(x|\underline{\psi}\right)_z$ with the benchmark $G\left(x|\underline{\psi}\right)_z$ of the results in (Volpe et al., 2019), we can identify

- Correctly classified scenarios: σ_x for which $G\left(x|\underline{\psi}\right)_z > (<)\, 0$ and $\hat{G}\left(x|\underline{\psi}\right)_z > (<)\, 0$.
- Misclassified scenarios: σ_x for which $G\left(x|\underline{\psi}\right)_z > (<) 0$ and $\hat{G}\left(x|\underline{\psi}\right)_z < (>) 0$.
- Critical scenarios: misclassified scenarios σ_x for which $\hat{G}\left(x|\underline{\psi}\right)_z > 0$ but $G\left(x|\underline{\psi}\right)_z < 0$.

In *Tables* 2-3, the $N = 32715$ seismic scenarios are accordingly divided in correctly classified, misclassified and critical scenarios for the metamodels built for the intensities $\underline{\psi} = 1, 1.3, 1.5, 1.8, 2.1, 2.5\ m$ in PoI $z = 2, 5, 8$ respectively.

z	2	2	2	2	2	2
$\underline{\psi}$	1	1.3	1.5	1.8	2.1	2.5
Correctly classified scenarios	31638	31852	32311	32398	32468	32603
Misclassified scenarios	1077	863	404	317	247	112
Critical scenarios	445	294	216	153	96	46

Table 2: correctly and misclassified scenarios for z=2

z	5	5	5	5	5	5
$\underline{\psi}$	1	1.3	1.5	1.8	2.1	2.5
Correctly classified scenarios	31571	31813	32207	32396	32461	32580
Misclassified scenarios	1144	902	508	319	254	135
Critical scenarios	432	327	227	163	109	52

Table 3: correctly and misclassified scenarios for z=5

z	8	8	8	8	8	8
$\underline{\psi}$	1	1.3	1.5	1.8	2.1	2.5
Correctly classified scenarios	30947	31551	31582	32108	32204	32496
Misclassified scenarios	1768	1164	1133	607	511	246
Critical scenarios	782	521	375	306	243	103

Table 4: correctly and misclassified scenarios for z=8

In *Figures* 17-19 the comparison between P-ds AK and the results of (Volpe et al., 2019) is reported plotting $\hat{G}\left(x|\underline{\psi}\right)_z\ vs.\ G\left(x|\underline{\psi}\right)_z$ for $\underline{\psi} = 1.8$ and $z = 2, 5, 8$, respectively. In the first and third quadrants, correctly classified scenarios are plotted in green ($G\left(x|\underline{\psi}\right)_z > (<)\ 0$ and $\hat{G}\left(x|\underline{\psi}\right)_z > (<)\ 0$), whereas in second and fourth quadrants, misclassified scenarios are reported in red ($\hat{G}\left(x|\underline{\psi}\right)_z > 0$ but $G\left(x|\underline{\psi}\right)_z < 0$ and $\hat{G}\left(x|\underline{\psi}\right)_z < 0$ but $G\left(x|\underline{\psi}\right)_z > 0$, respectively). Note that the misclassified scenarios are conservatively estimating $G\left(x|\underline{\psi}\right)_z$, being most of them laying in the second quadrant ($G\left(x|\underline{\psi}\right)_z > 0$ and $\hat{G}\left(x|\underline{\psi}\right)_z < 0$).

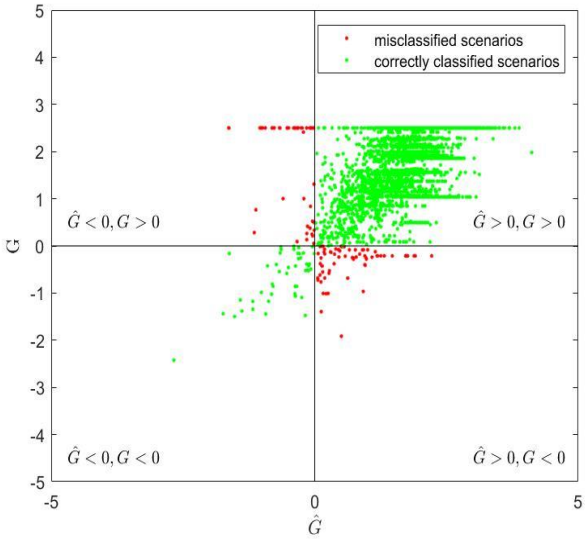

Figure 17: classification results for z=2 and $\bar{\psi}$=1.8

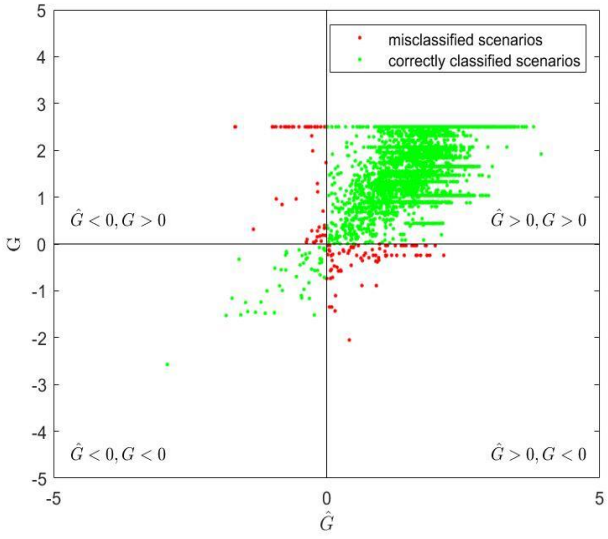

Figure 18: classification results for z=5 and $\bar{\psi}$=1.8

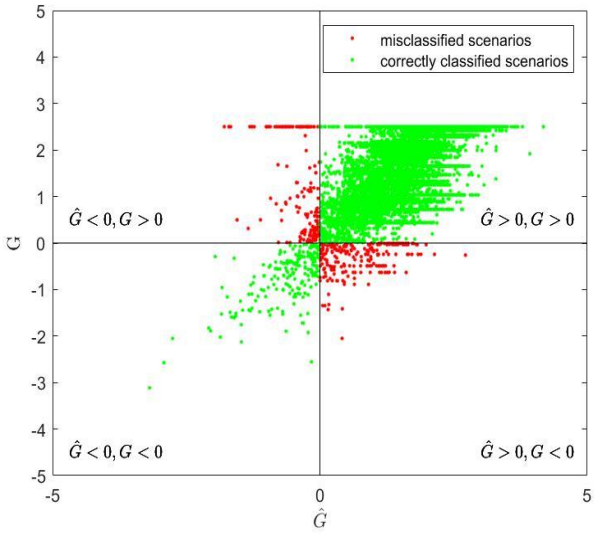

Figure 19: classification results for z=8 and $\bar{\psi}$=1.8

4.2 Coastal PoIs

The coastal PoIs $z = 2, 5, 8, 23, 64, 73, 88, 91, 94$ (*Figure* 20) are considered to highlight the dependencies of the P-ds AK based SPTHA on the local topography and hydrodynamics for points distributed along the coastline. This case study is relevant for the application of extended infrastructures, such as ports areas (Argyroudis et al. 2020), as well as for other typical risk mitigation actions which take place in extended areas (e.g., Tonini et al., 2021 and references therein).

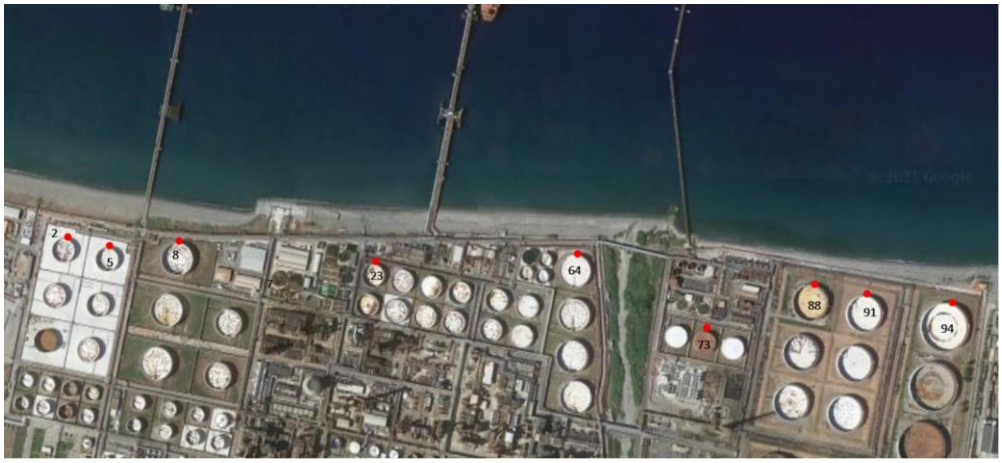

Figure 20: coastal PoIs

Figures 21 to 24 show, without loss of generality, the hazard curves for the PoI $z = 2, 5, 8, 23$, respectively: as before, our results are reported with continuous blue lines, whereas those obtained in (Volpe et al., 2019) with dashed red lines, and, for each PoI, the exceedance annual rate $\lambda\left(\psi_z \geq \underline{\psi}\right)$ and the error bars corresponding to the 15th and 85th percentiles are plotted. At the initial DoE of $\Delta = 256$, were added $\underline{K} = 360$ further seismic scenarios for a total of 616 belonging to $C = 318$ different clusters and consequent tsunami inundation simulations, as shown in *Table* 5. As already mentioned, the results in (Volpe et al., 2019) have been obtained with the run of $C = 613$ centroids simulations $\psi(x^c)_z$, each one taking approximately 30 [min] with 3 GPUs (i.e., the computational time is equal to 30 [min]*613 runs of the code=19390 [min]), whereas in this case the P-ds AK-based SPTHA results have been obtained running only $C = 318$ centroids simulations $\psi(x^c)_z$ (i.e., the computational time is equal to 80 [min] (for the Pds-AK training) + 30 [min]*318 runs of the code =9620 [min], again with a saving of about half of the time).

The estimated central values for the annual rates of exceedance $\lambda\left(\psi_z \geq \underline{\psi}\right)$ are here slightly underestimating the results of (Volpe et al., 2019) but, again, within the epistemic uncertainty bounds. Also, the uncertainty bounds, this time, show a slight underestimation, but overall, the P-ds AK-based approach provides a consistent picture of the hazard results, both in terms of central values (Root Mean Squared Error (RMSE) equal to [1.77E-6, 1.61E-6, 1.54E-6, 1.71E-6, 2.37E-6, 2.70E-7, 2.15E-6, 2.48E-6,2.34E-6] for $z = 2, 5, 8, 23, 64, 73, 88, 91, 94$, respectively) and epistemic uncertainty (error bars) and epistemic uncertainty (error bars).

	Pds-AK based SPTHA		Volpe et al. (2019)	
	Number of calls of seismic scenarios σ_x	Number of corresponding centroids (C)	Number of calls of seismic scenarios σ_x	Number of corresponding centroids (C)
Initial DoE (Δ)	256	36	/	/
Added DoE $(\underline{K})$	360	282	/	/
Total DoE	616	318	32715	613

Table 5: summary of the DoE and calls for coastal PoIs

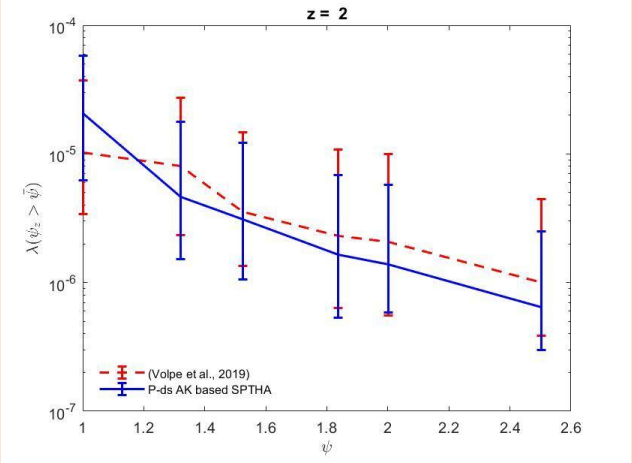

Figure 21: hazard curve for z=2

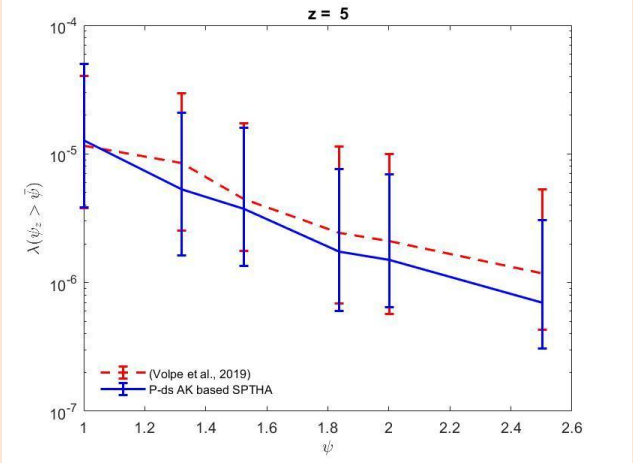

Figure 22: hazard curve for z=5

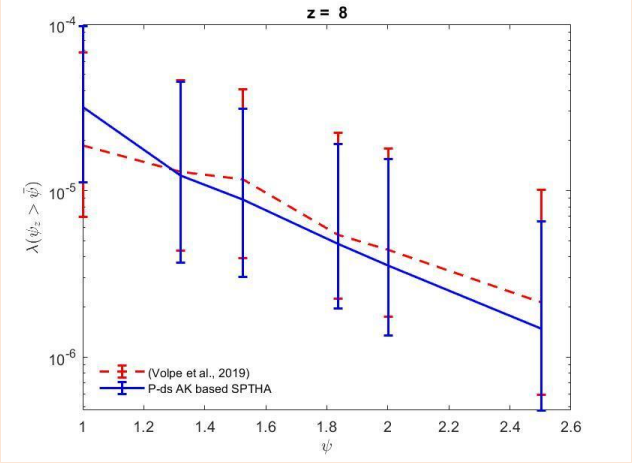

Figure 23: hazard curve for z=8

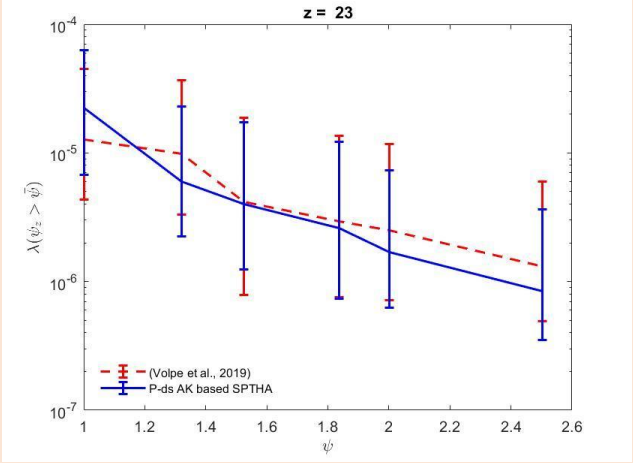

Figure 24: hazard curve for z=23

As above, the reduction of the number of centroids simulations $\psi(x^c)_z$ from $C = 613$ to $C = 318$ was made possible by the P-ds AK identification of the most critical seismic scenarios σ_x, i.e. those scenarios whose parameters x_j $(j = 1, \dots, J)$ would lead the simulation in the neighborhood of the limit state function $G\left(x|\underline{\psi}\right)_z = 0$. In the same fashion of Section 4.1, in *Figures* 25 to 32 are plotted, respectively, the distribution of the input parameters L, φ_{AB}, Strike, Dip and Rake, $E[\psi(x)_p], Var[\psi(x)_p]$ for all the available seismic scenarios (upper left), the initial DoE (upper right) and the added DoE (bottom).

The enrichment of scenarios is in line with the results of the concentrated points discussed in the previous Section. In particular, in *Figure 25* it can be seen that the P ds-AK has enriched the DoE with only relatively near seismic events with L between 0 and 200 km; in *Figure* 26 it can be seen that the P ds-AK

has enriched the DoE for angles φ_{AB} between 0° and 0.04°, the distribution of magnitudes (Figure 27) show an enrichment of seismic scenarios with Magnitude greater than 7.5 and lower than 8.

Figures 28 to *30* show that no changes in the DoE distribution are present for, respectively, the Rake, Stike and Dip angle with respect to the distribution of all seismic scenarios σ_x. Finally, in *Figures* 31-32, it can be seen that the P-ds AK has enriched the DoE with σ_x with high $E[\psi(x)_p]$, with a maximum around 6 meters, and high $Var[\psi(x)_p]$.

In conclusion, we can state that it is more likely that seismic scenarios in the neighborhood of $G\left(x|\underline{\psi}\right)_z = 0$ are close (low L) and in front (low φ_{AB}) to the site, with Magnitude between 7.5 and 8 and with a large and variable tsunami in the target coastal area. On the other hand, in this case study, Rake, Stike and Dip angles play a less relevant role for building the P-ds AK metamodels. Interestingly, Rake angle appears less relevant with respect to Section 4.1, probably connected to the greater geographic area spanned by the PoIs.

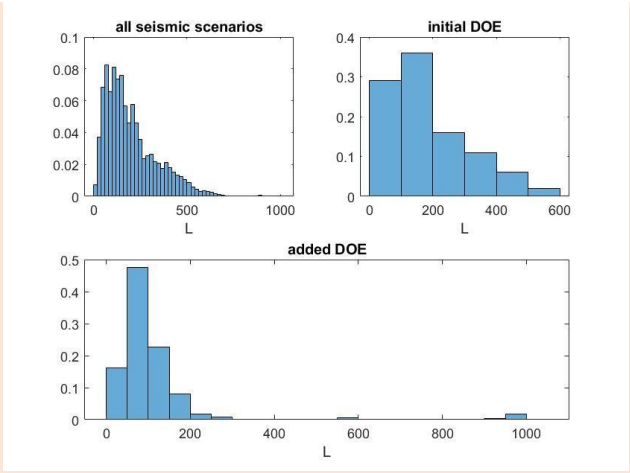

Figure 25: distributions of L

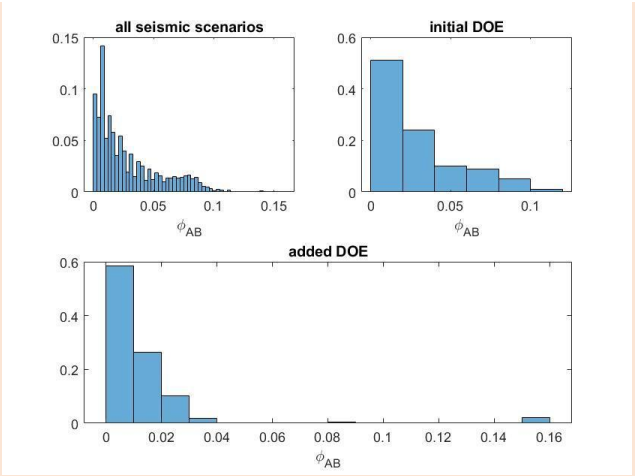

Figure 26: distributions of φ_{AB}

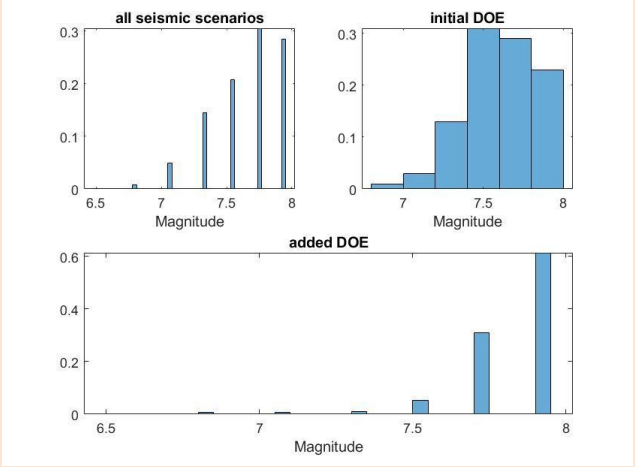

Figure 27: distributions of Magnitude

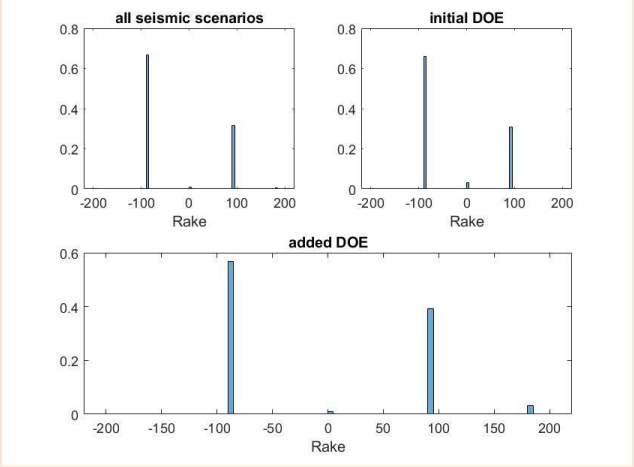

Figure 28: distributions of Rake

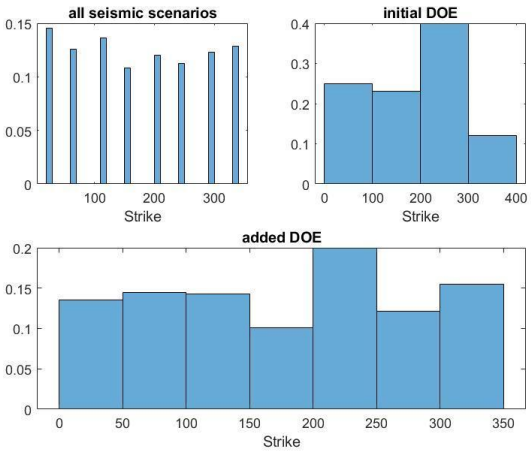

Figure 29: distributions of Strike

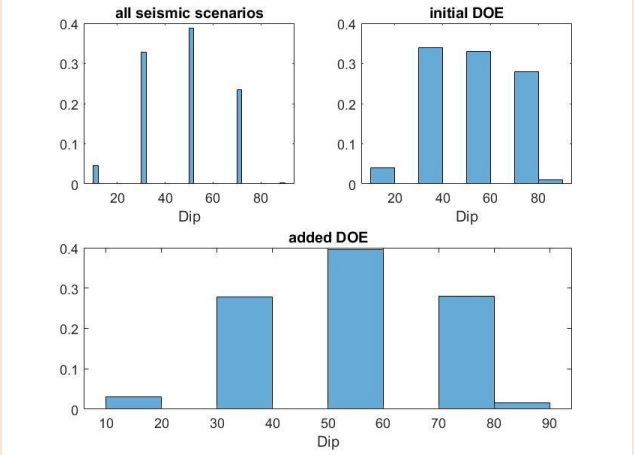

Figure 30: distributions of Dip

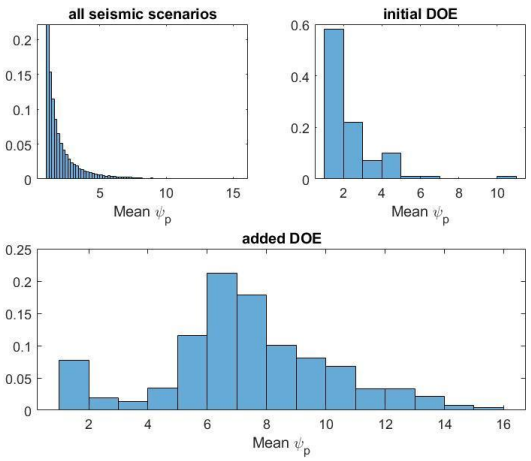

Figure 31: distributions of $\boldsymbol{E}[\boldsymbol{\psi}(\boldsymbol{x})_{\boldsymbol{p}}]$

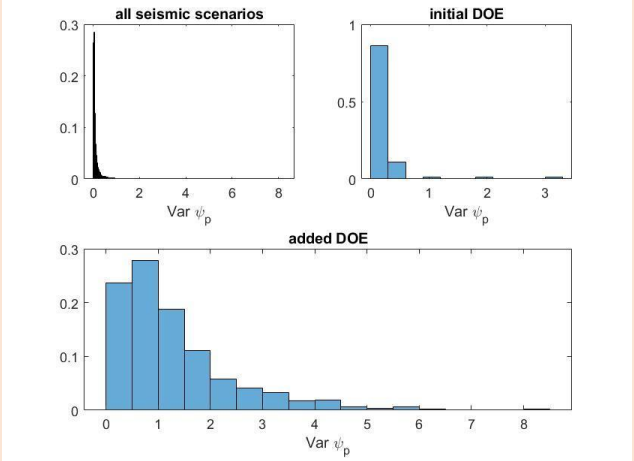

Figure 32: distributions of $\boldsymbol{Var}[\boldsymbol{\psi}(\boldsymbol{x})_{\boldsymbol{p}}]$

As in Section 4.1, In *Tables* 6-7 the division of the $N = 32715$ seismic scenarios in correctly classified, misclassified and critical scenarios is reported, for the metamodels built for the intensities $\underline{\psi} = 1, 1.3, 1.5, 1.8, 2.1, 2.5\ meters$ in PoI $z = 64, 91$, respectively.

z	64	64	64	64	64	64
$\underline{\psi}$	1	1.3	1.5	1.8	2.1	2.5
Correctly classified scenarios	30900	31761	31894	32411	32458	32627
Misclassified scenarios	1815	954	821	304	257	88
Underestimated scenarios	693	301	187	120	90	22

Table 6: correctly and incorrectly classified points for z=64

z	91	91	91	91	91	91
$\underline{\psi}$	1	1.3	1.5	1.8	2.1	2.5
Correctly classified scenarios	30807	31694	31905	32446	32494	32641
Misclassified scenarios	1908	1021	810	269	221	74
Underestimated scenarios	848	358	223	116	72	17

Table 7: correctly and incorrectly classified points for z=91

5 Conclusions

A novel P-ds-AK-based approach is proposed to reduce the computational effort related to the evaluation of the local SPTHA for safety critical systems like oil and gas and nuclear facilities. The SPTHA quantifies the probability that a tsunami wave caused by earthquakes exceeds a specific height in a specific place and time window. The approach is applied to the site of an oil refinery located in Milazzo, Sicily.

To account for the full variability of seismic triggering events, SPTHA must integrate the results of a large number of computationally demanding tsunami simulations, which can result an unfeasible task. To tackle this challenge, a four-steps approach has been proposed by Volpe et al (2019) to reduce the number of numerical simulations required. Here, we adopted a P-ds AK method as a further step to decrease the computational cost of the analysis, by identifying the seismic scenarios most affecting the hazard variability at specific target points, and then performing tsunami simulations only for a subset of the selected scenarios and using a metamodel for the others.

The approach turned out to be capable of accurately estimating the hazard curves, with a consistent reduction of the computational effort. We considered two case studies, both related a local SPTHA for the area of the oil refinery located in Milazzo (Sicily, Italy): a set of target points clustered in space around a few specific tanks exposed to the tsunami, and a set of coastal target points extending along the coast and covering the entire refinery. In both cases, the hazard curves produced by the reduced number of simulations are very close to the one obtained with a larger set of simulations, with central values well inside the estimated epistemic uncertainty. This is surely underestimated, as only uncertainty on the source is considered, while uncertainty on the inundation model could be very relevant too (e.g., Griffin et al., 2015; Song and Goda, 2021; Tonini et al. 2021). The P-ds AK procedure is able to correctly reproduce also the epistemic uncertainty bounds, showing that the computational cost reduction can be reached as well when epistemic uncertainty should be quantified. Note that the novel P-ds-AK-based approach proposed can be used on many areas of international relevance, like the coastal areas in the Mediterranean, including Eastern Sicily and Southern Creete in the Ionian Sea, Northern Sicily in the

Tyrrhenian Sea. Indeed, the approach extends that of Volpe et al. (2019), whose procedure has been successfully tested on such areas (Volpe et al. 2019; Argyroudis et al. 2020).

The developed P-ds AK procedure is limited to a few and relatively concentrated PoIs. This is the case of punctual or spatially concentrated infrastructures like coastal plants (e.g. nuclear power plants), where tsunami-sensitive areas are few and very concentrated. On the contrary, it is not applicable to other cases with a significant spatial extension, such as a near-coast railway network: future research should be directed towards increasing the number of points under study. We note that the entire chain of computation should be revised in this case, as also the classical approach to tsunami modelling adopting nested telescopic grids should be challenged.

On the other hand, whenever the target area is relatively limited (few kilometers), the limited number of tsunami inundation simulations necessary for this approach can be exploited to further improve the tsunami modelling approach and overcome some of present-day limitations. For example, it can lead to the adoption of more accurate tsunami modelling strategies, or to an enrichment of the source model to better explore source variability (e.g., including slip distribution), which in principle could lead to an increase in the number of clusters. All such improvements could lead to more accurate hazard results, compensating the increase of the computational demand, due to more advanced modelling, with the reduction of required simulations, due to the adoption of P-ds AK strategy. This is fundamental to plan mitigation and recovery strategies in case, for example, of NaTech events.

6 Acknowledgments

This study was developed within the research project “Assessment of Cascading Events triggered by the Interaction of Natural Hazards and Technological Scenarios involving the release of Hazardous Substances” funded by MIUR–- Italian Ministry for Scientific Research under the PRIN 2017 program (grant 2017CEYPS8).

Bibliography

Antonioni, G., Landucci, G., Necci, A., Gheorghiu, D., & Cozzani, V. (2015). *Quantitative assessment of risk due to NaTech scenarios caused by floods*. https://doi.org/10.1016/j.ress.2015.05.020

Argyroudis, S. A., Fotopoulou, S., Karafagka, S., Kyriazis Pitilakis, Selva, J., Salzano, E., Basco, A., Crowley, H., Rodrigues, D., Matos, J. P., Schleiss, A. J., Courage, W., Reinders, J., Cheng, Y., & Sinan. (2020). A risk-based multi-level stress test methodology: application to six critical non-nuclear infrastructures in Europe. *Natural Hazards*, *100*, 595–633. https://doi.org/10.1007/s11069-019-03828-5

Basili R, Brizuela B, Herrero A, Iqbal S, Lorito S, Maesano FE, Murphy S, Perfetti P, Romano F, Scala A, Selva J, Taroni M, Tiberti MM, Thio HK, Tonini R, Volpe M, Glimsdal S, Harbitz CB, Løvholt F, Baptista MA, Carrilho F, Matias LM, Omira R, Babeyko A, Hoechner A, Gürbüz M, Pekcan O, Yalçıner A, Canals M, Lastras G, Agalos A, Papadopoulos G, Triantafyllou I, Benchekroun S, Agrebi Jaouadi H, Ben Abdallah S, Bouallegue A, Hamdi H, Oueslati F, Amato A, Armigliato A, Behrens J, Davies G, Di Bucci D, Dolce M, Geist E, Gonzalez Vida JM, González M, Macías Sánchez J, Meletti C, Ozer Sozdinler C, Pagani M, Parsons T, Polet J, Power W, Sørensen M

and Zaytsev A (2021) The Making of the NEAM Tsunami Hazard Model 2018 (NEAMTHM18). Front. Earth Sci. 8:616594. doi: 10.3389/feart.2020.616594.

Behrens, J., Løvholt, F., Jalayer, F., Lorito, S., Salgado-Gálvez, M. A., Sørensen, M., Abadie, S., Aguirre-Ayerbe, I., Aniel-Quiroga, I., Babeyko, A., Baiguera, M., Basili, R., Belliazzi, S., Grezio, A., Johnson, K., Murphy, S., Paris, R., Rafliana, I., De Risi, R., … ˆ anoˇgluanoˇ anoˇglu, K. U. (2021). *Probabilistic Tsunami Hazard and Risk Analysis: A Review of Research Gaps*. *9*, 1. https://doi.org/10.3389/feart.2021.628772

Bouhlel, M. A., & Martins, J. R. R. A. (2017). *Gradient-enhanced kriging for high-dimensional problems*. https://arxiv.org/abs/1708.02663

Cruz, A. M., Franchello, G., & Krausmann, E. (2009). Assessment of Tsunami Risk to an Oil Refinery in Southern Italy. *JRC Scientific and Technical Reports*, 58. https://core.ac.uk/download/pdf/38613266.pdf

Echard, B., Gayton, N., & Lemaire, M. (2011). AK-MCS: An active learning reliability method combining Kriging and Monte Carlo Simulation. *Structural Safety*, *33*(2), 145–154. https://doi.org/10.1016/j.strusafe.2011.01.002

El-Hussain, I., Omira, R., Al-Habsi, Z., Baptista, M. A., Deif, A., & Mohamed, A. M. E. (2018). Probabilistic and deterministic estimates of near-field tsunami hazards in northeast Oman. *Geoscience Letters*, *5*, 30. https://doi.org/10.1186/s40562-018-0129-4

Gailler, A., Hébert, H., Schindelé, F., & Reymond, D. (2018). Coastal Amplification Laws for the French Tsunami Warning Center: Numerical Modeling and Fast Estimate of Tsunami Wave Heights Along the French Riviera. *Pure and Applied Geophysics*, *175*(4), 1429–1444. https://doi.org/10.1007/s00024-017-1713-9

Geist, E. L., & Parsons, T. (2014). *Undersampling power-law size distributions: effect on the assessment of extreme natural hazards*. *72*, 565–595. https://doi.org/10.1007/s11069-013-1024-0

Glimsdal, S., Løvholt, F., Harbitz, C. B., Romano, F., Lorito, S., Orefice, S., Brizuela, B., Selva, J., Hoechner, A., Volpe, M., Babeyko, A., Tonini, R., Wronna, M., & Omira, R. (2019). *A New Approximate Method for Quantifying Tsunami Maximum Inundation Height Probability*. https://doi.org/10.1007/s00024-019-02091-w

Grezio, A., Babeyko, A., Baptista, M. A., Behrens, J., Costa, A., Davies, G., Geist, E. L., Glimsdal, S., González, F. I., Griffin, J., Harbitz, C. B., LeVeque, R. J., Lorito, S., Løvholt, F., Omira, R., Mueller, C., Paris, R., Parsons, T., Polet, J., … Thio, H. K. (2017). Probabilistic Tsunami Hazard Analysis: Multiple Sources and Global Applications. *Reviews of Geophysics*, *55*(4), 1158–1198. https://doi.org/10.1002/2017RG000579

Iwabuchi, Y., Koshimura, S., & Imamura, F. (2006). Study on Oil Spread Caused by the 1964 Niigata Earthquake Tsunami. *Journal of Disaster Research*, *1*(1), 157–168. https://doi.org/10.20965/jdr.2006.p0157

Jian, W., Zhili, S., Qiang, Y., & Rui, L. (2017). Two accuracy measures of the Kriging model for structural reliability analysis. *Reliability Engineering and System Safety*, *167*, 1339–1351. https://doi.org/10.1016/j.ress.2017.06.028

Kameshwar S., Cox D.T., Barbosa A.R., Farokhnia K., Park H., Alam M.S., van de Lindt J.W.(2019). Probabilistic decision-support framework for community resilience: Incorporating multi-hazards, infrastructure interdependencies, and resilience goals in a Bayesian network. *Reliability Engineering and System Safety*, Volume 191, November 2019, Article number 106568.

Kaufman L. and Rousseeuw, P. J. (2009). *Finding Groups in Data: An Introduction*. John Wiley & Sons, Inc.

Khakzad N. and Cozzani V. (2020). Special issue: Quantitative assessment and risk management of Natech accidents. *Reliability Engineering and System Safety*, Volume 203, November 2020 Article number 107198.

L. Puppo A. Bersano, C. Bertani, F. Di Maio, N. Pedroni, E. Z. (2021). Failure Identification in a Nuclear Passive Safety System by Monte Carlo Simulation with Adaptive Kriging. *Nuclear Engineering and Design*.

Lan M., Gardoni P., Qin, R., Zhang X., Zhu J., Lo, S. "Modeling Natech-related domino effects in process clusters: a network-based approach", *Reliability Engineering and System Safety*, 221, article number 108329 (2022).

Landucci, G., Antonioni, G., Tugnoli, A., & Cozzani, V. (2012). Release of hazardous substances in flood events: Damage model for atmospheric storage tanks. *Reliability Engineering and System Safety*, *106*, 200–216. https://doi.org/10.1016/j.ress.2012.05.010

Liu, H., Ong, Y. S., & Cai, J. (2018). A survey of adaptive sampling for global metamodeling in support of simulation-based complex engineering design. *Structural and Multidisciplinary Optimization*, *57*(1), 393–416. https://doi.org/10.1007/s00158-017-1739-8

Lo, C.K., Pedroni, N., Zio, E., (2014). Treating uncertainties in a nuclear seismic probabilistic risk assessment by means of the Dempster-Shafer theory of evidence. *Nuclear Engineering and Technology*, Volume 46, Issue 1, Pages 11 – 262014.

Løvholt, F, Griffin, J., & Salgado-Gálvez, M. A. (2016). Tsunami Hazard and Risk Assessment on the Global Scale. In R.

A. Meyers (Ed.), *Encyclopedia of Complexity and Systems Science* (pp. 1–34). Springer Berlin Heidelberg. https://doi.org/10.1007/978-3-642-27737-5_642-1

Macias, J., Castro, M. J., Ortega, S., Escalante, C., Manuel, J., & Gonza´gonza´lez-Vida, G. (2017). Performance Benchmarking of Tsunami-HySEA Model for NTHMP's Inundation Mapping Activities. *Pure and Applied Geophysics*, *174*. https://doi.org/10.1007/s00024-017-1583-1

Mebarki, A., Jerez, S., Prodhomme, G., & Reimeringer, M. (2016). Natural hazards, vulnerability and structural resilience: tsunamis and industrial tanks. *Geomatics, Natural Hazards and Risk*, *7*, 5–17. https://doi.org/10.1080/19475705.2016.1181458

Marzocchi, W., Iervolino, I., Giorgio, M., Falcone, G. (2015) When Is the Probability of a Large Earthquake Too Small? *Seismological Research Letters Volume 86, Number 6 November/December 2015.*

Mesa-Gomez, A., Casal, J., & MuNoz, F. (2020). Risk analysis in Natech events: State of the art. *Journal of Loss Prevention in the Process Industries*, *64*, 104071. https://doi.org/10.1016/j.jlp.2020.104071

Molinari, I., Tonini, R., Lorito, S., Piatanesi, A., Romano, F., Melini, D., Hoechner, A., Gonzàlez Vida, J. M., Maciás, J., Castro, M. J., & de la Asunción, M. (2016). Fast evaluation of tsunami scenarios: uncertainty assessment for a Mediterranean Sea database. *Natural Hazards and Earth System Sciences*, *16*(12), 2593–2602. https://doi.org/10.5194/nhess-16-2593-2016

Moreno, V. C., Ricci, F., Sorichetti, R., Misuri, A., & Cozzani, V. (2019). Analysis of Past Accidents Triggered by Natural Events in the Chemical and Process Industry. *Chemical Engineering Transactions*, *74*, 1405–1410. https://doi.org/10.3303/CET1974235

Prasad, R. (2012). Tsunami hazard assessment at nuclear power plant sites in the United States of America. In *Tsunami Hazard Assessment at U.S. Nuclear Power Plants*.

Raymond H. Myers, Douglas C. Montgomery, C. M. A.-C. (2016). *Response Surface Methodology: Process and Product Optimization Using Designed Experiments* (Wiley (ed.)).

Sato, A., & Lyamzina, Y. (2018). *Diversity of Concerns in Recovery after a Nuclear Accident: A Perspective from Fukushima*. https://doi.org/10.3390/ijerph15020350

Sinharay, S., Continuous Probability Distributions, in International Encyclopedia of Education (Third Edition), Elsevier, ISBN 978-0-08-044894-7, 2010.

Selva, J., Tonini, R., Molinari, I., Tiberti, M. M., Romano, F., Grezio, A., Melini, D., Piatanesi, A., Basili, R., & Lorito, S. (2016). Quantification of source uncertainties in Seismic Probabilistic Tsunami Hazard Analysis (SPTHA). *Geophysical Journal International Geophys. J. Int*, *205*, 1780–1803. https://doi.org/10.1093/gji/ggw107

Selva J , Amato A, Armigliato A, Basili R, Bernardi F, Brizuela B, Cerminara M, de' Micheli Vitturi M, Di Bucci D, Di Manna P, Esposti Ongaro T, Lacanna G, Lorito S, Løvholt F, Mangione D, Panunzi E, Piatanesi A, Ricciardi A, Ripepe M, Romano F, Santini M, Scalzo A, Tonini R, Volpe M, Zaniboni F (2021), Tsunami risk management for crustal earthquakes and non-seismic sources in Italy. , La Rivista del Nuovo Cimento 44: 69-144, DOI : https://doi.org/10.1007/s40766-021-00016-9

Sun, Z., Wang, J., Li, R., & Tong, C. (2017). LIF: A new Kriging based learning function and its application to structural reliability analysis. *Reliability Engineering and System Safety*, *157*, 152–165. https://doi.org/10.1016/j.ress.2016.09.003

Tabajdeh A., Sharma N, Gardoni P., "Uncertainty propagation in risk and resilience analysis of hierarchical systems", Reliability Engineering and System Safety, 219, 108208 (2022).

Teixeira, R., Nogal, M., O'Connor, A., & Martinez-Pastor, B. (2020). Reliability assessment with density scanned adaptive Kriging. *Reliability Engineering and System Safety*, *199*, 106908. https://doi.org/10.1016/j.ress.2020.106908

Tinti, S, Tonini, R., Bressan, L., Armigliato, A., Gardi, A., Guillande, R., Valencia, N., & Scheer, S. (2011). Handbook of Tsunami Hazard and Damage Scenarios. In *Sciences-New York*. https://doi.org/10.2788/21259

Tonini, R., Armigliato, A., Pagnoni, G., Zaniboni, F., & Tinti, S. (2011). Tsunami hazard for the city of Catania, eastern Sicily, Italy, assessed by means of Worst-case Credible Tsunami Scenario Analysis (WCTSA). *Natural Hazards and Earth System Science*, *11*(5), 1217–1232. https://doi.org/10.5194/nhess-11-1217-2011

Tonini, Roberto, Di Manna, P., Lorito, S., Selva, J., Volpe, M., Romano, F., Basili, R., Brizuela, B., Castro, M. J., de la Asunción, M., Di Bucci, D., Dolce, M., Garcia, A., Gibbons, S. J., Glimsdal, S., González-Vida, J. M., Løvholt, F., Macías, J., Piatanesi, A., … Bucci, D. D. (2021). *Testing Tsunami Inundation Maps for Evacuation Planning in Italy*. *9*, 11. https://doi.org/10.3389/feart.2021.628061

Turati, P., Pedroni, N., & Zio, E. (2017). Simulation-based exploration of high-dimensional system models for

identifying unexpected events. *Reliability Engineering and System Safety*, *165*, 317–330. https://doi.org/10.1016/j.ress.2017.04.004

Volpe, M., Lorito, S., Selva, J., Tonini, R., Romano, F., & Brizuela, B. (2019). From regional to local SPTHA: efficient computation of probabilistic tsunami inundation maps addressing near-field sources. *Natural Hazards and Earth System Sciences*, *19*(3), 455–469. https://doi.org/10.5194/nhess-19-455-natech

Wang, Z., & Wang, P. (2013). A Maximum Confidence Enhancement Based Sequential Sampling Scheme for Simulation-Based Design. *Journal of Mechanical Design*, *136*(2). https://doi.org/10.1115/1.4026033

Zhang, Xiaobo, Lu, Z., & Cheng, K. (2021). AK-DS: An adaptive Kriging-based directional sampling method for reliability analysis. *Mechanical Systems and Signal Processing*, *156*, 107610. https://doi.org/10.1016/j.ymssp.2021.107610

Zhang, Xufang, Wang, L., & Sørensen, J. D. (2019). REIF: A novel active-learning function toward adaptive Kriging surrogate models for structural reliability analysis. *Reliability Engineering and System Safety*, *185*, 440–454. https://doi.org/10.1016/j.ress.2019.01.014